

Large Bayesian Tensor Autoregressions

Yaling Qi

Purdue University

November 6, 2025

Abstract

The availability of multidimensional economic datasets has grown significantly in recent years. An example is bilateral trade values across goods among countries, comprising three dimensions—importing countries, exporting countries, and goods—forming a third-order tensor time series. This paper introduces a general Bayesian tensor autoregressive framework to analyze the dynamics of large, multidimensional time series with a particular focus on international trade across different countries and sectors. Departing from the standard homoskedastic assumption in this literature, we incorporate flexible stochastic volatility into the tensor autoregressive models. The proposed models could capture time-varying volatility due to the COVID-19 pandemic and recent outbreaks of war. To address computational challenges and mitigate overfitting, we develop an efficient sampling method based on low-rank Tucker decomposition and hierarchical shrinkage priors. Additionally, we provide a factor interpretation of the model showing how the Tucker decomposition projects large-dimensional disaggregated trade flows onto global factors.

JEL classification: C11, C32, C55

Keywords: tensor, Tucker decomposition, tensor autoregressions, stochastic volatility, shrinkage prior

1 Introduction

Recent years have seen the proliferation of big data across biological, physical, economic, and financial fields, which provides unprecedented access to diverse multidimensional datasets, including, but not limited to, increasingly structured and complex high-dimensional time-series data. Many can be viewed as matrices; for example, cross-region panel datasets consisting of state-level macroeconomic indices; the dynamic bilateral trade volumes between countries can be treated as matrix-variate time series. More generally, higher-dimensional time-series datasets can be organized as tensors. In the global economy, multi-commodity dynamic trade values among countries can be characterized by three dimensions—importing countries, exporting countries, and goods—forming a third-order array, also known as a tensor time series.

Early studies tend to directly stack the high-dimensional data into a long vector and apply vector autoregressions (VAR) or factor models to analyze the large data. However, this approach has some limitations. First, this transformation disregards the inherent structural information within the datasets. In the trade example, we can expect cross-sectional dependencies between different countries and goods. Although previous research has extended the standard VAR framework to account for interdependencies between countries—for instance, through panel VAR (Canova and Ciccarelli, 2013) or global VAR (Pesaran, Schuermann, and Weiner, 2004; Dees, Mauro, Pesaran, and Smith, 2007; Bussière, Chudik, and Sestieri, 2009)—these models allow for cross-sectional interdependencies or global linkages. However, they remain limited to aggregate trade values at the country level, thereby overlooking the disaggregated multilateral and multi-category trade distribution across countries. Moreover, analyzing such networks involves handling hundreds or even tens of thousands of time series, making traditional VAR models extremely time-consuming or even infeasible due to their substantial computational complexity (Bańbura, Giannone, and Reichlin, 2010; Koop, 2013; Carriero, Clark, and Marcellino, 2015).

Recent studies have started to explore multidimensional economic datasets while preserving the structure in both responses and predictors. Many of them focus on lower-dimensional matrix-variate regressions, including both autoregressive and factor models (Hoff, 2015; Ding and Dennis Cook, 2018; Chen, Xiao, and Yang, 2021; Chan and Qi, 2025; Wang, Liu, and Chen, 2019; Chen, Tsay, and Chen, 2020; Zhang, 2024). Some

matrix autoregressive models assume a bilinear form with two coefficient matrices. The two transition matrices are often interpreted as capturing either column-wise or row-wise interactions, depending on the data. These studies provide deeper insights into cross-sectional dependencies or spillovers.

By contrast, third-order tensor regressions still remain rare. One major concern in tensor regressive models is the "curse of dimensionality", which arises when high-dimensional models involve a great number of parameters. This leads to two major estimation issues. On the one hand, the tensor structure of predictors and responses typically involves a large number of free parameters, which significantly increases computational complexity in high-dimensional settings. The estimation process even becomes particularly infeasible when handling datasets comprising thousands of time series. On the other hand, if the number of unknown parameters far exceeds the available time periods, accurate estimation becomes very difficult without regularization. To address this, previous Bayesian research has often employed hierarchical shrinkage priors, which could help improve estimation and inference efficiency by shrinking negligible elements toward zero.

To overcome these challenges, a widely used approach is tensor decomposition, which utilizes the assumption of low multi-linear rank in a tensor. This method extends the concept of Singular Value Decomposition (SVD) from matrices to higher-order tensors, enabling more efficient computation.

Two widely used tensor decomposition methods are the PARAFAC/CANDECOMP (CP) decomposition (Harshman et al., 1970; Carroll and Chang, 1970) and the Tucker decomposition (Tucker, 1963; Levin, 1965; Tucker, 1966). CP decomposition breaks down the multidimensional coefficient tensor into a sum of rank-one tensors, each constructed as the outer product of marginal vectors along each dimension. This approach reduces millions of elements in the coefficient tensor to a manageable number for efficient and reliable estimation.

Tucker decomposition extends the CP decomposition by representing a tensor as a core tensor multiplied by factor matrices along each mode. Compared to CP decomposition, Tucker decomposition is more flexible as it allows for different ranks across dimensions and capture more complicate associations among marginals. Importantly, CP decomposition can be viewed as a special case of Tucker decomposition (see Section 2.5), where the core tensor is superdiagonal, and the ranks are the same across all dimensions (Kolda and

Bader, 2009).

Most of the existing tensor regression literature is designed to handle either tensor-valued predictors or responses—such as in scalar-on-tensor, vector-on-tensor, or their reverse settings (Zhou, Li, and Zhu, 2013; Zhou, Bhattacharya, Herring, and Dunson, 2015; Rabusseau and Kadri, 2016; Guhaniyogi, Qamar, and Dunson, 2017; Lock, 2018). Zhou, Li, and Zhu (2013) recognize the limitations of traditional methods in analyzing complex, multidimensional medical imaging data and propose generalized linear tensor regressive models based on CP decomposition to accommodate tensor-valued covariates. Li, Xu, Zhou, and Li (2018) extend their framework by modeling the coefficient tensor using Tucker decomposition instead of CP. However, the Lasso-regularized estimation approach in Zhou, Li, and Zhu (2013) has a limitation, as it depends heavily on manually selected tuning parameters. To address this, Guhaniyogi, Qamar, and Dunson (2017) develop a Bayesian framework incorporating a novel class of multiway shrinkage priors, which naturally induce sparsity and enable reliable identification of important coefficients. Subsequently, Spencer, Guhaniyogi, and Prado (2020) extend this framework by introducing rank-specific prior scale parameters through a stick-breaking construction, allowing for efficient shrinkage across ranks of CP decomposition.

In comparison, the research on tensor-on-tensor regressive models is still scarce. Hoff (2015) introduces a general multilinear tensor regressive framework to analyze social networks in the context of tensor-valued longitudinal and multivariate relational data. More recently, Billio, Casarin, Iacopini, and Kaufmann (2023) extend the scalar-on-tensor model of Guhaniyogi, Qamar, and Dunson (2017) to a more general tensor-on-tensor setting, applying it to a two-layer network of trade and credit linkages among ten countries and deriving the corresponding impulse response functions.

Moreover, Tucker decomposition is rarely explored in the tensor-on-tensor regressive literature, except for Wang, Zheng, and Li (2024), and Wang and Xu (2024). Wang, Zheng, and Li (2024) introduces both convex and non-convex estimation methods for tensor autoregressive models with the Tucker decomposition. They also show an additional advantage of Tucker decomposition over CP decomposition which facilitates dynamic factor interpretations of the multilinear model. Wang and Xu (2024) propose an efficient MCMC method for jointly estimating model dimensions and parameters. In contrast, we focus on a more general framework capable of accommodating a variety of stochastic volatilities

and global-local shrinkage priors.

Our paper contributes to the development of more general Bayesian Tensor Autoregressions in three key directions. First, we incorporate stochastic volatility into the model to account for time-varying volatility, as a growing body of literature recognizes its importance for estimation and inference in macroeconomic models — whether small- or large-scale VARs— particularly during extreme periods such as the global financial crisis, the COVID-19 pandemic, and major geopolitical conflicts (Cogley and Sargent, 2005; Sims and Zha, 2006; Koop and Korobilis, 2013; Carriero, Clark, Marcellino, and Mertens, 2022; Chan, 2023). We also incorporate a specialized hierarchical shrinkage prior—an adapted version of the multiway stick-breaking shrinkage prior proposed in Guhaniyogi (2020) for the CP decomposition—to induce parameter sparsity and enhance the reliability of the estimation.

Regarding the second contribution, we illustrate it in two parts. First, we develop a more efficient Bayesian estimation method to handle large datasets in a parsimonious manner. Our framework is particularly well suited to high-dimensional settings—for example, a third-order tensor \mathcal{Y}_t of size $20 \times 20 \times 10$ contains 4,000 elements. Moreover, we extend the commonly used CP decomposition to a more flexible Tucker decomposition. Unlike CP, Tucker models allow for different ranks both within and across responses and predictors, and introduce a core tensor that facilitates modeling interactions among the marginals. This added flexibility enables the model to capture more nuanced and complex predictive relationships.

The final contribution lies in the interpretation of the Tucker model. We view the Tucker decomposition as using loading matrices to project higher-dimensional data onto lower-dimensional factors. Moreover, most response and predictor factor series align with aggregate global indicators. This factor interpretation provides deeper insight into the Tucker decomposition and its economic content.

The rest of the paper is structured as follows: the next section introduces the flexible framework for autoregressive tensor models. Section 3 outlines the multiway shrinkage priors and provides details of posterior computation under Tucker decomposition. Section 4 presents Monte Carlo simulation results comparing various competing methods under a range of data-generating processes. Section 5 applies the proposed efficient estimation method to analyze the multi-category international bilateral trade flows. Finally, section

6 concludes the paper and discusses potential directions for further research.

2 A Flexible Framework for Tensor Autoregressive Models

We propose a general framework for Bayesian Tensor Autoregressions with stochastic volatility that mitigates the substantial computational burden via tensor decomposition. This approach enables efficient modeling of high-dimensional time series while flexibly accommodating a range of time-varying error structures.

2.1 Tensor Algebra

We first introduce some basic and important tensor notation and algebra. More details can be found in Kolda and Bader (2009).

A tensor is a multidimensional array. A first-order tensor is a vector (denoted by boldface lowercase letters, e.g., \mathbf{x}), a second-order tensor is a matrix (denoted by boldface Euler script letters, e.g., \mathbf{X}), and tensors of order three or higher are referred to as higher-order tensors (denoted by boldface Euler script letters, e.g., \mathcal{X}).

The mode- n matricization of a tensor $\mathcal{X} \in \mathbb{R}^{I_1 \times I_2 \times \dots \times I_N}$ is denoted by $\mathcal{X}_{(n)}$ with size $I_n \times \prod_{i \neq n} I_i$, and arranges the mode- n fibers to be the columns of the resulting matrix. Tensor element (i_1, i_2, \dots, i_N) maps to matrix element (i_n, j) , where $j = 1 + \sum_{k \neq n} (i_k - 1) J_k$, with $J_k = \prod_{m \neq n}^{k-1} I_m$.

The generalized inner product of two different-sized tensors $\mathcal{X} \in \mathbb{R}^{I_1 \times \dots \times I_n \times \dots \times I_N}$ and $\mathcal{Y} \in \mathbb{R}^{I_n \times \dots \times I_N}$ is the sum of the products of their corresponding entries, resulting in an $n - 1$ th-order tensor of dimension $I_1 \times \dots \times I_{n-1}$, whose (i_1, \dots, i_{n-1}) -th element is given by:

$$\langle \mathcal{X}, \mathcal{Y} \rangle_{i_1, \dots, i_{n-1}} = \sum_{i_n=1}^{I_n} \dots \sum_{i_N=1}^{I_N} \mathcal{X}_{i_1, \dots, i_{n-1}, i_n, \dots, i_N} \mathcal{Y}_{i_n, \dots, i_N}.$$

2.2 Introduction to Tensor Autoregressive Models

Consider a third-order tensor time series $\{\mathcal{Y}_t\}_{t=1}^T$ of size $I_1 \times I_2 \times I_3$. The evolution of \mathcal{Y}_t is captured by the following tensor autoregressive (TAR) model of lag order p :

$$\mathcal{Y}_t = \mathcal{A}_t + \sum_{j=1}^p \langle \mathcal{B}_j, \mathcal{Y}_{t-j} \rangle + \mathcal{E}_t \quad (1)$$

where \mathcal{Y}_{t-j} , \mathcal{A}_t and \mathcal{E}_t are all third-order tensors of size $I_1 \times I_2 \times I_3$, and \mathcal{B}_j is a sixth-order tensor of size $I_1 \times I_2 \times I_3 \times I_1 \times I_2 \times I_3$. The operator $\langle \cdot, \cdot \rangle$ denotes the generalized inner product between two tensors. \mathcal{A}_t captures the intercepts or deterministic trends; for example, it can represent a linear time trend in \mathcal{Y}_t , expressed as $\mathcal{A}_0 + \mathcal{A}_1 t$ over time. Elementwise, let $\mathcal{Y}_{t,i_1,i_2,i_3}(\mathcal{E}_{t,i_1,i_2,i_3})$ be the $(i_1, i_2, i_3)^{th}$ element of $\mathcal{Y}_t(\mathcal{E}_t)$, then

$$\mathcal{Y}_{t,i_1,i_2,i_3} = \mathcal{A}_{t,i_1,i_2,i_3} + \sum_{j=1}^p \sum_{i_4=1}^{I_1} \sum_{i_5=1}^{I_2} \sum_{i_6=1}^{I_3} \mathcal{B}_{j,i_1,i_2,i_3,i_4,i_5,i_6} \mathcal{Y}_{t-j,i_4,i_5,i_6} + \mathcal{E}_{t,i_1,i_2,i_3} \quad (2)$$

The lagged effect of $\mathcal{Y}_{t-j,i_4,i_5,i_6}$ on $\mathcal{Y}_{t,i_1,i_2,i_3}$ is given by $\mathcal{B}_{j,i_1,i_2,i_3,i_4,i_5,i_6}$. If we want to study the dynamics of bilateral trade among n countries across m commodity categories, we can represent the data as an $n \times n \times m$ tensor-valued \mathcal{Y}_t , where $\mathcal{Y}_{t,i_1,i_2,i_3}$ denotes the import value of country i_1 from the exporting country i_2 for commodity category i_3 at time t . The first dimension correspond to importing countries, the second dimension to exporting countries, and the third dimension to industries or commodity categories.

As for the error term \mathcal{E}_t , we assume \mathcal{E}_t follows a conditionally Gaussian distribution with Kronecker structure:

$$\text{vec}(\mathcal{E}_t) \sim \mathcal{N}(\mathbf{0}_I, \mathbf{\Sigma}), \text{ where } \mathbf{\Sigma} = \mathbf{\Sigma}_3 \otimes \mathbf{\Sigma}_2 \otimes \mathbf{\Sigma}_1 \quad (3)$$

where $I = I_1 I_2 I_3$, and $\text{vec}(\mathcal{E}_t) = \text{vec}(\mathbf{E}_{t,(1)})$, with $\text{vec}(\mathbf{X})$ denoting the operation that stacks the columns of the matrix \mathbf{X} vertically into a single vector. $\mathbf{\Sigma}_1$, $\mathbf{\Sigma}_2$, and $\mathbf{\Sigma}_3$ are $I_1 \times I_1$, $I_2 \times I_2$, and $I_3 \times I_3$ covariance matrices, respectively. The Kronecker structure is adopted to achieve dimensionality reduction. Without this structure, sampling $\mathbf{\Sigma}$ would require estimating $\mathcal{O}(I^2)$ free parameters, making estimation unreliable with

limited samples and computationally expensive—or even infeasible—as I increases, especially in high-dimensional tensor time series. In contrast, imposing a Kronecker structure drastically reduces the number of free parameters to $\sum_{i=1}^6 I_i R_i$ and lowers the computational cost to $\mathcal{O}(\max(I_1, I_2, I_3)^6)$, thereby making the estimation more reliable and computationally tractable even in high-dimensional settings. To sample Σ_i , we first compute the mode- i matricization of the tensor \mathcal{E}_t , denoted by $\mathbf{E}_{t,(i)}$. It can be readily shown that $\mathbf{E}_{t,(i)}$ satisfies the following property:

$$\text{vec}(\mathbf{E}_{t,(i)}) \sim \mathcal{N}(\mathbf{0}, \tilde{\Sigma}_i) \quad (4)$$

where $\tilde{\Sigma}_1 = \Sigma_3 \otimes \Sigma_2 \otimes \Sigma_1$, $\tilde{\Sigma}_2 = \Sigma_3 \otimes \Sigma_1 \otimes \Sigma_2$, and $\tilde{\Sigma}_3 = \Sigma_2 \otimes \Sigma_1 \otimes \Sigma_3$.

2.3 Relation to VARs

The Tensor Autoregressive (TAR) model can be expressed in the form of a Vector Autoregressive (VAR) model, where each VAR coefficient matrix $\hat{\mathbf{B}}_j \in \mathbb{R}^{I \times I}$ corresponds to a reshaped version of the coefficient tensor \mathcal{B}_j , such that $\text{vec}(\hat{\mathbf{B}}_j) = \text{vec}(\mathcal{B}_j)$. Specifically, the TAR model can be written as:

$$\text{vec}(\mathcal{Y}_t) = \text{vec}(\mathcal{A}_t) + \sum_{j=1}^p \hat{\mathbf{B}}_j \text{vec}(\mathcal{Y}_{t-j}) + \text{vec}(\mathcal{E}_t) \quad (5)$$

The covariance matrix of $\text{vec}(\mathcal{E}_t)$ in Equation (3) admits a meaningful interpretation. The error matrix specified in Equation (4) can be expressed through its mode- i matricizations as:

$$\mathbf{E}_{t,(1)} = \Sigma_1^{1/2} \mathbf{Z}_{1t} (\Sigma_3 \otimes \Sigma_2)^{1/2}, \quad \mathbf{E}_{t,(2)} = \Sigma_2^{1/2} \mathbf{Z}_{2t} (\Sigma_3 \otimes \Sigma_1)^{1/2}, \quad \mathbf{E}_{t,(3)} = \Sigma_3^{1/2} \mathbf{Z}_{3t} (\Sigma_2 \otimes \Sigma_1)^{1/2},$$

where \mathbf{Z}_{1t} , \mathbf{Z}_{2t} , and \mathbf{Z}_{3t} are matrices of dimensions $I_1 \times (I_2 I_3)$, $I_2 \times (I_1 I_3)$, and $I_3 \times (I_1 I_2)$, respectively, each consisting of independent standard normal entries. This formulation highlights that Σ_1 , Σ_2 , and Σ_3 represent the covariance matrices along the first, second, and third tensor modes, respectively. More generally, the covariance between the (i_1, j_1, k_1) and (i_2, j_2, k_2) elements of \mathcal{E}_t is given by:

$$\text{Cov}(e_{t,i_1,j_1,k_1}, e_{t,i_2,j_2,k_2}) = \sigma_{1,i_1,i_2} \sigma_{2,j_1,j_2} \sigma_{3,k_1,k_2}$$

2.4 Stochastic Volatility

Previous studies have demonstrated the importance of modeling time-varying volatility in high-dimensional macroeconomic settings (Koop and Korobilis, 2013; Carriero, Clark, and Marcellino, 2016b, 2019; Chan, Eisenstat, Hou, and Koop, 2020; Chan, 2023), especially during periods of heightened uncertainty such as the global financial crisis and the COVID-19 pandemic. Building on the framework proposed by Chan and Qi (2025), this paper introduces a generalized approach that accommodates two types of stochastic volatility processes via a mixture parameter, ω_t . The distribution of the error term \mathcal{E}_t given the latent variable ω_t can be expressed as follows:

$$\text{vec}(\mathcal{E}_t) \sim \mathcal{N}(\mathbf{0}_I, \omega_t \mathbf{\Sigma}), \text{ where } \mathbf{\Sigma} = \mathbf{\Sigma}_3 \otimes \mathbf{\Sigma}_2 \otimes \mathbf{\Sigma}_1 \quad (6)$$

If $\omega_t = 1$ for all t , the model reduces to a homoskedastic volatility setting. Two key examples within this framework are recognition of outlier and common stochastic volatility (CSV).

In the first example, we account for potential outliers using the explicit outlier component proposed by Stock and Watson (2016). Specifically, we define $\omega_t = o_t^2$, where o_t is either a point mass at 1 or follows a uniform distribution over the interval (2, 10). When $o_t = 1$, the economy is in a normal state, whereas when $o_t \geq 2$, economic uncertainty increases, which we classify as an outlier state, capturing periods of abnormal volatility or structural disruptions. The sampling algorithm for ω_t is detailed in the appendix of Chan and Qi (2025).

Additionally, the common stochastic volatility (CSV) model, originally proposed by Carriero, Clark, and Marcellino (2016a), assumes that log-volatility, $h_t = \log(\omega_t)$, follows a stationary AR(1) process:

$$h_t = \phi h_{t-1} + \varepsilon_t$$

where $\varepsilon_t \sim N(0, \sigma^2)$, $|\phi| < 1$ and the initial condition is defined as $h_1 \sim (0, \sigma^2/(1 - \phi^2))$. Under this AR(1) specification, volatility at time t strongly depends on previous periods, leading to more persistent effects of past volatility in the CSV model.

2.5 Tensor Decompositions

For the rest of the paper, we focus on the TAR(1) model and simplify the notation by letting \mathcal{B} represent \mathcal{B}_1 . The transition tensor \mathcal{B} consists of I^2 free parameters, where $I = I_1 I_2 I_3$. For example, if $I_1 = I_2 = 20$ and $I_3 = 10$, I would be 4,000, resulting in tens of millions (16,000,000) of parameters to estimate, which is computationally infeasible. To overcome this challenge, we adopt tensor decomposition, a widely used dimensionality reduction technique for high-dimensional tensors. Tensor decomposition is a higher-order generalization of matrix singular value decomposition (SVD).

Let \mathbf{M} be an $m \times n$ matrix of rank R with singular value decomposition (SVD) $(\mathbf{U}, \mathbf{D}, \mathbf{V})$. Then we have

$$\mathbf{M} = \mathbf{U}\mathbf{D}\mathbf{V}' = \sum_{\ell=1}^R d_{\ell} \mathbf{u}_{\ell} \mathbf{v}_{\ell}^{\top},$$

where \mathbf{D} is a diagonal matrix with diagonal entries d_{ℓ} for $\ell = 1, \dots, R$, and \mathbf{U} and \mathbf{V} are orthogonal matrices whose columns correspond to the left and right singular vectors, \mathbf{u}_{ℓ} and \mathbf{v}_{ℓ} , respectively. The term $\mathbf{u}_{\ell} \mathbf{v}_{\ell}^{\top}$ denotes the outer product of \mathbf{u}_{ℓ} and \mathbf{v}_{ℓ} —that is, the $m \times n$ matrix whose (i, j) -th entry equals $\mathbf{u}_{\ell}(i) \mathbf{v}_{\ell}(j)$. Hence, any rank- R matrix can be expressed as a sum of R rank-one matrices:

$$\mathbf{M} = d_1 \mathbf{u}_1 \mathbf{v}_1^{\top} + \dots + d_R \mathbf{u}_R \mathbf{v}_R^{\top}$$

Furthermore, the partial sum $\sum_{\ell=1}^r d_{\ell} \mathbf{u}_{\ell} \mathbf{v}_{\ell}^{\top}$ provides the best rank- r approximation to \mathbf{M} in the sense of minimizing the Frobenius norm of the approximation error.

The two most common tensor decomposition methods are the CP decomposition and the Tucker decomposition. CP decomposition (Harshman et al., 1970; Carroll and Chang, 1970) extends the concept of SVD to higher-order tensors by approximating a high-dimensional tensor as the sum of R rank-one tensors, where each rank-one tensor is the outer product of marginal vectors across all dimensions. Specifically,

$$\mathcal{B} \approx \sum_{r=1}^R \mathbf{b}_1^r \circ \mathbf{b}_2^r \circ \mathbf{b}_3^r \circ \mathbf{b}_4^r \circ \mathbf{b}_5^r \circ \mathbf{b}_6^r \quad (7)$$

Figure 1 below illustrates the CP decomposition.

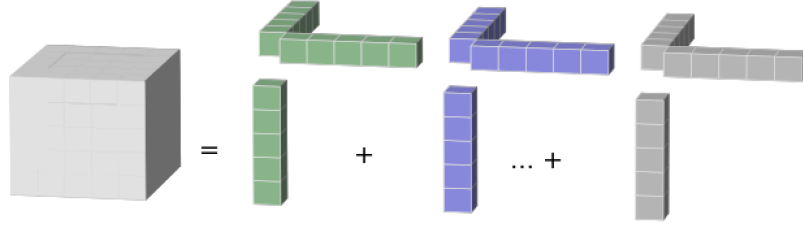


Figure 1: Visualization of three-dimensional CP Decomposition

In Billio, Casarin, Iacopini, and Kaufmann (2023), the tensor-valued predictor is stacked into a long vector, resulting in a fourth-order coefficient tensor whose final dimension equals to the product of the predictor dimensions. Specifically, if the tensor data has dimensions $I_1 \times I_2 \times I_3$, this leads to a computational complexity of $O(I^3)$, where $I = \prod_{i=1}^3 I_i$. In contrast, we preserve the tensor structure of the predictors and employ a sixth-order coefficient tensor of dimension $I_1 \times I_2 \times I_3 \times I_1 \times I_2 \times I_3$, reducing the computational complexity to $O(\max_i(I_i^3))$.

Tucker decomposition is a generalization of CP decomposition. It was first proposed by Tucker (1963), with further refinements made in later works such as Levin (1965) and Tucker (1966). Tucker decomposition breaking down a tensor into a core tensor coupled with factor matrices along each mode. Specifically, given a sixth-order tensor $\mathcal{B} \in \mathbb{R}^{I_1 \times I_2 \times I_3 \times I_1 \times I_2 \times I_3}$, it can be written as

$$\mathcal{B} \approx \sum_{r_1=1}^{R_1} \cdots \sum_{r_6=1}^{R_6} g_{r_1, \dots, r_6} \mathbf{b}_1^{r_1} \circ \cdots \circ \mathbf{b}_6^{r_6} = \llbracket \mathcal{G} ; \mathbf{B}_1, \dots, \mathbf{B}_6 \rrbracket \quad (8)$$

In the first equation, \mathcal{B} is approximated by a sum of $R_p = \prod_{i=1}^6 R_i$ rank-one tensors. For notational convenience, the second equation adopts a more compact form, denoted by $\llbracket \mathcal{G}; \mathbf{B}_1, \dots, \mathbf{B}_6 \rrbracket$, as introduced in Kolda and Bader (2009). $\mathbf{B}_i = (\mathbf{b}_i^1, \dots, \mathbf{b}_i^{R_i})$, $i = 1, \dots, 6$, containing R_i marginal vectors, where R_i is viewed as the rank of dimension

i . \mathbf{B}_i works as the factor matrix representing the principal components in i^{th} dimension. Specifically, the marginal vectors $\mathbf{b}_1^{r_1}, \mathbf{b}_4^{r_4} \in \mathbb{R}^{I_1}$, $\mathbf{b}_2^{r_2}, \mathbf{b}_5^{r_5} \in \mathbb{R}^{I_2}$, and $\mathbf{b}_3^{r_3}, \mathbf{b}_6^{r_6} \in \mathbb{R}^{I_3}$, with r_i ranging from 1 to R_i . One major advantage of Tucker decomposition over CP decomposition is its ability to allow different ranks along each dimension.

The tensor $\mathcal{G} \in \mathbb{R}^{R_1 \times \dots \times R_6}$ is referred to as the low rank core tensor, where its entries indicate the level of interaction among the various components. CP decomposition can be considered a special case of Tucker decomposition, where the core tensor is superdiagonal and the ranks are identical across all modes. In contrast, the core tensor in Tucker decomposition can capture more complex structured information from the original tensor.

Since $R_i \leq I_i$ for all i , the core tensor \mathcal{G} serves as a compressed representation of the original tensor \mathcal{B} . CP and Tucker decomposition thus reduce the number of free parameters in \mathcal{B} from I^2 to $2 \sum_{i=1}^3 I_i R$ and $R_p + \sum_{i=1}^6 I_i R_i$, respectively, where $I = \prod_{i=1}^3 I_i$ and $R_p = \prod_{i=1}^6 R_i$. For instance, in the earlier trade example with $I_1 = I_2 = 20$ and $I_3 = 10$, CP and Tucker decomposition reduce the number of free parameters from millions to hundreds.

2.6 Identification Issue

Although the coefficient tensor \mathcal{B} in equation (1) is identifiable, its Tucker decomposition in equation (8) is not. The lack of uniqueness arises from the following factors:

1. Scale Indeterminacy: If there exists a set of scalars $\{\lambda, \lambda_1^{r_1}, \dots, \lambda_6^{r_6}\}$, where r_i ranges from 1 to R_i , such that $\lambda \prod_{i=1}^6 \lambda_i^{r_i} = 1$ for any combination of $\{r_i\}_{i=1}^6$, then replacing \mathcal{G} with $\lambda \mathcal{G}$ and $\mathbf{b}_i^{r_i}$ with $\lambda_i^{r_i} \mathbf{b}_i^{r_i}$ results in the same decomposition.

2. Rotational Indeterminacy: For any rotation of \mathbf{B}_i (multiplied by an $R_i \times R_i$ rotation matrix on right side), if we rotate \mathcal{G} inversely along mode- i , the decomposition remains unchanged. Let me illustrate this with a simple example. Consider the previous example of an $m \times n$ matrix \mathbf{M} of rank R (a second-order tensor). In this case, the SVD would be one possible solution to the Tucker decomposition, as mentioned earlier,

$$\mathbf{M} = \mathbf{U} \mathbf{D} \mathbf{V}'$$

where \mathbf{U} and \mathbf{V} are the factor matrices for the first and second dimensions, respectively, and \mathbf{S} is the core matrix for \mathbf{M} . Given two non-singular matrices \mathbf{P}_1 and \mathbf{P}_2 , we can create a new pair of factor matrices: $\tilde{\mathbf{U}} = \mathbf{U}\mathbf{P}_1^{-1}$, $\tilde{\mathbf{V}} = \mathbf{V}\mathbf{P}_2^{-1}$. Next, we apply an inverse rotation to the core matrix \mathbf{S} along each dimension: $\tilde{\mathbf{S}} = \mathbf{P}_1\mathbf{S}\mathbf{P}_2'$. This gives us another Tucker decomposition for \mathbf{M} , since

$$\tilde{\mathbf{U}}\tilde{\mathbf{S}}\tilde{\mathbf{V}}' = (\mathbf{U}\mathbf{P}_1^{-1})(\mathbf{P}_1\mathbf{S}\mathbf{P}_2')(\mathbf{V}\mathbf{P}_2^{-1})' = \mathbf{U}\mathbf{S}\mathbf{V}' = \mathbf{M}.$$

Thus, we obtain an equivalent Tucker decomposition, showing that the decomposition is not unique due to the rotation indeterminacy.

Despite the challenges due to scale and rotation indeterminacy, applying higher-order singular value decomposition (HOSVD) to the estimated posterior mean of the coefficient tensor \mathcal{B} yields a structured decomposition with several desirable properties, as discussed in (De Lathauwer, De Moor, and Vandewalle, 2000; Kolda and Bader, 2009; Wang, Zheng, and Li, 2024). Through HOSVD, the new factor matrix $\bar{\mathbf{B}}_i$ that contains the top R_i left singular vectors of $\mathbf{B}_{(i)}$ is column orthonormal, that is, $\bar{\mathbf{B}}_i'\bar{\mathbf{B}}_i = \mathbf{I}_{R_i}$. Furthermore, the core tensor $\bar{\mathcal{G}}$ is all-orthogonal, meaning $\bar{\mathbf{G}}_{(i)}\bar{\mathbf{G}}_{(i)}^\top$ is a diagonal matrix for $i = 1, \dots, 6$. The all-orthogonality property serves an analogous role to the diagonality property in matrix SVD. In a sense, the HOSVD estimates can be viewed as the best rank- R_i approximation to \mathcal{B} in terms of the Frobenius norm over its i^{th} two-dimensional projection.

Although HOSVD estimates are still not unique due to potential sign indeterminacy, they have greatly mitigated the identification issue and are sufficient for our interpretation in several aspects. We can also use the projection matrices of these factor matrices, $\mathbf{B}_i\mathbf{B}_i'$, to resolve the sign indeterminacy, as demonstrated in Wang, Zheng, and Li (2024).

3 Bayesian Estimation

In this section, we discuss the estimation procedure for efficiently sampling parameters in BTAR models using Markov chain Monte Carlo (MCMC) techniques under Tucker decomposition, of which CP decomposition is a special case obtained by fixing the core tensor to be superdiagonal. Before analyzing the sampling algorithm, we first introduce the hierarchical shrinkage priors which naturally induce sparsity in the parameters.

3.1 Global-local Shrinkage Priors

The prior distribution on the Tucker marginal vectors plays a key role in shrinking some negligible elements toward zero and thereby improving the efficiency of estimation and inference. A widely used class for high-dimensional problems is hierarchical shrinkage. Specifically, we adapt the multiway stick-breaking (SB) shrinkage prior of Guhaniyogi (2020) from the CP decomposition to the Tucker framework, allowing the shrinkage to act on the margins. Because the prior enables shrinkage across ranks through a stick-breaking structure for the rank-specific parameters, we do not perform explicit rank selection; instead, the shrinkage mechanism naturally favors a low-rank structure.

In the prior specification, we assume that the r_i^{th} marginal vector of mode i follows a hierarchical distribution as a normal mixture centered at 0:

$$\mathbf{b}_i^{r_i} \sim N(0, \tau_i \phi_i^{r_i} \mathbf{I}_{I_i})$$

The global parameters τ_i regulate the shrinkage level of the R_i margins of i^{th} dimension, and the rank-specific parameters $\{\phi_i^{r_i}\}_{i=1}^6$ control shrinkage across ranks. Specifically, $\phi_i^{r_i}$ follows a stick-breaking distribution, where the sum of $\phi_i^{r_i}$ across r_i equals 1.

$$\begin{aligned} \tau_i &\sim \text{Gamma}(\alpha_{\tau_i}, \beta_{\tau_i}), \\ \phi_i^{r_i} &= \eta_i^{r_i} \prod_{l=1}^{r_i-1} (1 - \eta_i^l) \text{ for } r_i = 1, \dots, R_i - 1, \\ \phi_i^{R_i} &= \prod_{l=1}^{R_i-1} (1 - \eta_i^l), \text{ where } \eta_i^{r_i} \stackrel{iid}{\sim} \text{Beta}(1, \alpha_i) \end{aligned}$$

Conditional on $\phi_i^{r_i}$, $\mathbf{b}_i^{r_i}$ follows a normal-gamma distribution. The marginal prior distribution of $\mathbf{b}_i^{r_i}$ has heavier tails than Gaussian distribution. The stick-breaking prior imposes increasing shrinkage across ranks, promoting a low-rank and parsimonious representation. It relies on the finite stick-breaking construction for the local parameters $\phi_i^{r_i}$, where smaller α_i values drive $\phi_i^{r_i}$ towards 0. Each α_i is drawn from a discrete uniform grid and updated via a greedy Gibbs sampler. The posterior distributions of these shrinkage parameters are provided in Appendix B.

3.2 Posterior Computation

In this subsection, we develop a unified framework for estimating the parameters of the TAR model— $\mathbf{B} = (\mathbf{B}_1, \dots, \mathbf{B}_6)$, \mathcal{G} , $\boldsymbol{\Sigma} = (\boldsymbol{\Sigma}_1, \boldsymbol{\Sigma}_2, \boldsymbol{\Sigma}_3)$, and $\boldsymbol{\omega} = (\omega_1, \dots, \omega_T)$. We describe the sampling procedure for \mathbf{B}_1 , \mathbf{B}_4 , and $\boldsymbol{\Sigma}$ in the main text, while additional details on the samplers for the remaining parameters are provided in Appendix B.

Based on the covariance structure in equation (4), the likelihood function can be expressed as

$$P(\mathcal{Y} \mid \mathcal{B}, \boldsymbol{\Sigma}, \boldsymbol{\omega}) = (2\pi)^{-\frac{TI}{2}} \mid \boldsymbol{\Sigma}_3 \otimes \boldsymbol{\Sigma}_2 \mid^{-\frac{TI_1}{2}} \mid \boldsymbol{\Sigma}_1 \mid^{-\frac{TI_2 I_3}{2}} \\ \times \prod_{t=1}^T \omega_t^{-\frac{I}{2}} \exp \left[-\frac{1}{2\omega_t} \text{tr} \left((\boldsymbol{\Sigma}_3 \otimes \boldsymbol{\Sigma}_2)^{-1} \mathbf{E}'_{t,(1)} \boldsymbol{\Sigma}_1^{-1} \mathbf{E}_{t,(1)} \right) \right] \quad (9)$$

where $\mathbf{E}_{t,(1)}$ is the mode-1 matricization of the tensor \mathcal{E}_t .

Lemma 1. *As stated in Section 3 of Kolda and Bader (2009), the mode- i matricization of \mathcal{B} satisfies the following equation.*

$$\mathbf{B}_{(i)} = \mathbf{B}_i \mathbf{G}_{(i)} (\mathbf{B}_6 \otimes \dots \otimes \mathbf{B}_{i+1} \otimes \mathbf{B}_{i-1} \otimes \dots \otimes \mathbf{B}_1)' = \mathbf{B}_i \mathbf{G}_{(i)} \mathbf{B}'_{-i} \quad (10)$$

where $\mathbf{G}_{(i)}$ denotes the mode- i matricization of \mathcal{G} , and $\mathbf{B}_{-i} = \mathbf{B}_6 \otimes \dots \otimes \mathbf{B}_{i+1} \otimes \mathbf{B}_{i-1} \otimes \dots \otimes \mathbf{B}_1$.

Proposition 1. *Let $\mathbf{Y}_{t,(i)}$ denote the mode- i matricization of \mathcal{Y}_t and $\mathbf{X}_{it} = \mathbf{y}_{t-1} \otimes \mathbf{I}_{k_i}$ where $k_i = \prod_{j \neq i} I_j$, then the following equations hold:*

$$\mathbf{Y}_{t,(i)} = \mathbf{A}_{t,(i)} + \mathbf{B}_i \mathbf{G}_{(i)} \mathbf{B}'_{-i} \mathbf{X}_{it} + \mathbf{E}_{t,(i)}, \quad i = 1, 2, 3 \quad (11)$$

The proof of this proposition is given in Appendix A. This proposition allows to transform the tensor autoregressions into multiple bilinear matrix regressions. The likelihood function in the first equation of (9) can be rewritten as:

$$P(\mathcal{Y} \mid \mathbf{B}_1, \mathbf{B}_{-1}, \boldsymbol{\Sigma}, \boldsymbol{\omega}) = (2\pi)^{-\frac{TI}{2}} \mid \boldsymbol{\Sigma}_3 \otimes \boldsymbol{\Sigma}_2 \mid^{-\frac{TI_1}{2}} \mid \boldsymbol{\Sigma}_1 \mid^{-\frac{TI_2 I_3}{2}} \\ \times \prod_{t=1}^T \omega_t^{-\frac{I}{2}} \exp \left[-\frac{1}{2\omega_t} \text{tr} \left((\boldsymbol{\Sigma}_3 \otimes \boldsymbol{\Sigma}_2)^{-1} (\mathbf{Y}_{t,(1)} - \mathbf{A}_{t,(1)} - \mathbf{B}_1 \mathbf{G}_{(1)} \mathbf{B}'_{-1} \mathbf{X}_{1t})' \boldsymbol{\Sigma}_1^{-1} (\mathbf{Y}_{t,(1)} - \mathbf{A}_{t,(1)} - \mathbf{B}_1 \mathbf{G}_{(1)} \mathbf{B}'_{-1} \mathbf{X}_{1t}) \right) \right] \quad (12)$$

Consider the normally distributed prior for $\mathbf{B}_i, i = 1, 2, 3$, for example,

$$\text{vec}(\mathbf{B}_i) \sim \mathcal{N}(\mathbf{b}_{i0}, \mathbf{V}_{\mathbf{b}_i})$$

where $\mathbf{b}_{i0} = \mathbf{0}$ and $\mathbf{V}_{\mathbf{b}_i} = \text{diag}(\tau_i \phi_i^1 \mathbf{I}_{I_i}, \dots, \tau_i \phi_i^{R_i} \mathbf{I}_{I_i})$ is an $I_i R_i \times I_i R_i$ diagonal matrix of shrinkage prior variances. Then $(\text{vec}(\mathbf{B}_1) \mid \mathbf{Y}, \mathbf{B}_{-1}, \mathbf{G}_1, \boldsymbol{\Sigma}, \boldsymbol{\omega})$ has the following normal distribution:

$$(\text{vec}(\mathbf{B}_1) \mid \mathbf{Y}, \mathbf{B}_{-1}, \mathbf{G}_1, \boldsymbol{\Sigma}, \boldsymbol{\omega}) \sim \mathcal{N}(\hat{\mathbf{b}}_1, \mathbf{K}_{\mathbf{b}_1}^{-1}) \quad (13)$$

where

$$\begin{aligned} \mathbf{K}_{\mathbf{b}_1} &= \mathbf{V}_{\mathbf{b}_1}^{-1} + \sum_{t=1}^T (\omega_t^{-1} \mathbf{G}_{(1)} \mathbf{B}'_{-1} \mathbf{X}_{1t} (\boldsymbol{\Sigma}_3^{-1} \otimes \boldsymbol{\Sigma}_2^{-1}) \mathbf{X}'_{1t} \mathbf{B}_{-1} \mathbf{G}'_{(1)}) \otimes \boldsymbol{\Sigma}_1^{-1} \\ \hat{\mathbf{b}}_1 &= \mathbf{K}_{\mathbf{b}_1}^{-1} \left(\mathbf{V}_{\mathbf{b}_1}^{-1} \mathbf{b}_{10} + \sum_{t=1}^T \text{vec}(\omega_t^{-1} (\boldsymbol{\Sigma}_1^{-1} \mathbf{Y}_{t,(1)} - \mathbf{A}_{t,(1)}) (\boldsymbol{\Sigma}_3^{-1} \otimes \boldsymbol{\Sigma}_2^{-1}) \mathbf{X}'_{1t} \mathbf{B}_{-1} \mathbf{G}'_{(1)}) \right) \end{aligned}$$

Similarly, we have shown in Appendix B that $(\mathbf{B}_2 \mid \mathbf{Y}, \mathbf{B}_{-2}, \mathbf{G}_2, \boldsymbol{\Sigma}, \boldsymbol{\omega})$ and $(\mathbf{B}_3 \mid \mathbf{Y}, \mathbf{B}_{-3}, \mathbf{G}_3, \boldsymbol{\Sigma}, \boldsymbol{\omega})$ also follow a Gaussian distribution.

Next, we discuss the posterior distributions of $\mathbf{B}_4, \mathbf{B}_5$, and \mathbf{B}_6 , which are more tricky. We primarily focus on \mathbf{B}_4 in the main text, while the sampling procedures for \mathbf{B}_5 and \mathbf{B}_6 are provided in Appendix B. The first step is to separate \mathbf{B}_4 from the other factor matrices, which can be achieved through the following lemma.

Lemma 2. *Let $\mathbf{y}_t = \text{vec}(\mathcal{Y}_t)$, $\mathbf{a}_t = \text{vec}(\mathcal{A}_t)$, and $\mathbf{e}_t = \text{vec}(\mathcal{E}_t)$. Then, we have*

$$\mathbf{y}_t = \mathbf{a}_t + \tilde{\mathbf{B}}_m \tilde{\mathbf{G}} \tilde{\mathbf{B}}' \mathbf{y}_{t-1} + \mathbf{e}_t = \mathbf{a}_t + \tilde{\mathbf{B}}_m \tilde{\mathbf{G}} ((\mathbf{B}'_6 \otimes \mathbf{B}'_5) \mathbf{Y}'_{t-1,(1)} \otimes \mathbf{I}_{R_4}) \text{vec}(\mathbf{B}'_4) + \mathbf{e}_t \quad (14)$$

where $\tilde{\mathbf{B}}_m = \mathbf{B}_3 \otimes \mathbf{B}_2 \otimes \mathbf{B}_1$, $\tilde{\mathbf{B}} = \mathbf{B}_6 \otimes \mathbf{B}_5 \otimes \mathbf{B}_4$. $\tilde{\mathbf{G}}$ is an $\tilde{R}_m \times \tilde{R}$ matrix satisfying $\text{vec}(\tilde{\mathbf{G}}) = \text{vec}(\mathcal{G})$, where $\tilde{R}_m = R_1 R_2 R_3$ and $\tilde{R} = R_4 R_5 R_6$. The proof of this lemma is given in Appendix A.

Suppose the prior on $\text{vec}(\mathbf{B}'_4)$ is given by a Gaussian distribution, $\text{vec}(\mathbf{B}'_4) \sim \mathcal{N}(\mathbf{b}_4^0, \mathbf{V}_{\mathbf{b}_4})$, where \mathbf{b}_4^0 is a zero vector of dimension $I_1 R_4$, and $\mathbf{V}_{\mathbf{b}_4}$ is an $I_1 R_4 \times I_1 R_4$ diagonal matrix with shrinkage prior variances. Then the posterior distribution of $\text{vec}(\mathbf{B}'_4)$ is as follows:

$$\left(\text{vec}(\mathbf{B}'_4)|\mathbf{Y}, \tilde{\mathbf{B}}_m, \mathbf{B}_5, \mathbf{B}_6, \tilde{\mathbf{G}}, \boldsymbol{\Sigma}\right) \sim \mathcal{N}(\hat{\mathbf{b}}_4, \mathbf{K}_{\mathbf{b}_4}^{-1})$$

where

$$\begin{aligned} \mathbf{K}_{\mathbf{b}_4} &= \mathbf{V}_{\mathbf{b}_4}^{-1} + \sum_{t=1}^T \frac{1}{\omega_t} (\mathbf{Y}_{t-1,(1)}(\mathbf{B}_6 \otimes \mathbf{B}_5) \otimes \mathbf{I}_{R_4}) \tilde{\mathbf{G}}' \tilde{\mathbf{B}}'_m \boldsymbol{\Sigma}^{-1} \tilde{\mathbf{B}}_m \tilde{\mathbf{G}} ((\mathbf{B}'_6 \otimes \mathbf{B}'_5) \mathbf{Y}'_{t-1,(1)} \otimes \mathbf{I}_{R_4}) \\ \hat{\mathbf{b}}_4 &= \mathbf{K}_{\mathbf{b}_4}^{-1} \left(\mathbf{V}_{\mathbf{b}_4}^{-1} \mathbf{b}_4^0 + \sum_{t=1}^T \frac{1}{\omega_t} (\mathbf{Y}_{t-1,(1)}(\mathbf{B}_6 \otimes \mathbf{B}_5) \otimes \mathbf{I}_{R_4}) \tilde{\mathbf{G}}' \tilde{\mathbf{B}}'_m \boldsymbol{\Sigma}^{-1} (\mathbf{y}_t - \mathbf{a}_t) \right) \end{aligned}$$

The full conditional distribution for $(\mathbf{B}'_5|\mathbf{Y}, \tilde{\mathbf{B}}_m, \mathbf{B}_4, \mathbf{B}_6, \tilde{\mathbf{G}}, \boldsymbol{\Sigma})$ and $(\mathbf{B}'_6|\mathbf{Y}, \tilde{\mathbf{B}}_m, \mathbf{B}_4, \mathbf{B}_5, \tilde{\mathbf{G}}, \boldsymbol{\Sigma})$ are provided in Appendix B.

Finally, with respect to sampling \mathcal{G} , we need to revisit the Lemma 2. Considering the stacked form of the first equation by defining $\mathbf{Y} = [\mathbf{y}_1, \dots, \mathbf{y}_T]$, $\mathbf{A} = [\mathbf{a}_1, \dots, \mathbf{a}_T]$, $\mathbf{X} = [\mathbf{y}_0, \dots, \mathbf{y}_{T-1}]$, and $\mathbf{E} = [\mathbf{e}_1, \dots, \mathbf{e}_T]$, then we have

$$\mathbf{Y} = \mathbf{A} + \tilde{\mathbf{B}}_m \tilde{\mathbf{G}} \tilde{\mathbf{B}}' \mathbf{X} + \mathbf{E}$$

where $\tilde{\mathbf{B}} = \mathbf{B}_6 \otimes \mathbf{B}_5 \otimes \mathbf{B}_4$, $\tilde{\mathbf{B}}_m = \mathbf{B}_3 \otimes \mathbf{B}_2 \otimes \mathbf{B}_1$ and $\tilde{\mathbf{G}}$ is an $\tilde{R}_m \times \tilde{R}$ matrix satisfying $\text{vec}(\tilde{\mathbf{G}}) = \text{vec}(\mathcal{G})$. In addition, by vectorizing both sides, we obtain:

$$\mathbf{y} = \mathbf{a} + \left(\mathbf{X}' \tilde{\mathbf{B}} \otimes \tilde{\mathbf{B}}_m\right) \text{vec}(\tilde{\mathbf{G}}) + \mathbf{e} = \mathbf{a} + \left(\mathbf{X}' \tilde{\mathbf{B}} \otimes \tilde{\mathbf{B}}_m\right) \text{vec}(\mathcal{G}) + \mathbf{e} \quad (15)$$

where $\mathbf{y} = [\mathbf{y}'_1, \dots, \mathbf{y}'_T]'$, $\mathbf{a} = [\mathbf{a}'_1, \dots, \mathbf{a}'_T]'$, $\mathbf{e} = [\mathbf{e}'_1, \dots, \mathbf{e}'_T]'$. Suppose the prior on $\text{vec}(\mathcal{G})$ is given by $\text{vec}(\mathcal{G}) \sim \mathcal{N}(\mathbf{g}_0, \mathbf{V}_{\mathbf{g}})$, where \mathbf{g}_0 is an R dimensional vector, and $\mathbf{V}_{\mathbf{g}}$ is an $R \times R$ diagonal matrix. Then the posterior distribution of $\text{vec}(\mathcal{G})$ is given as follows:

$$\left(\text{vec}(\mathcal{G})|\mathbf{Y}, \tilde{\mathbf{B}}_m, \tilde{\mathbf{B}}, \boldsymbol{\Sigma}\right) \sim \mathcal{N}(\hat{\mathbf{g}}, \mathbf{K}_{\mathbf{g}}^{-1})$$

where

$$\begin{aligned} \mathbf{K}_{\mathbf{g}} &= \mathbf{V}_{\mathbf{g}}^{-1} + \left(\tilde{\mathbf{B}}' \mathbf{X} \boldsymbol{\Omega}^{-1} \mathbf{X}' \tilde{\mathbf{B}}\right) \otimes \left(\tilde{\mathbf{B}}'_m \boldsymbol{\Sigma}^{-1} \tilde{\mathbf{B}}_m\right) \\ \hat{\mathbf{g}} &= \mathbf{K}_{\mathbf{g}}^{-1} \left(\mathbf{V}_{\mathbf{g}}^{-1} \mathbf{g}_0 + \text{vec}(\tilde{\mathbf{B}}'_m \boldsymbol{\Sigma}^{-1} (\mathbf{Y} - \mathbf{A}) \boldsymbol{\Omega}^{-1} \mathbf{X}' \tilde{\mathbf{B}})\right) \end{aligned}$$

Regarding the estimation of covariance matrices $\Sigma_i, i = 1, 2, 3$, if we assume that Σ_i follows an inverse Wishart prior distribution, $\Sigma_i \sim \mathcal{IW}(\nu_i, \mathbf{S}_{i0})$, then the posterior distribution of Σ_i is still an inverse Wishart distribution as below:

$$\Sigma_i \sim \mathcal{IW}\left(\nu_i + TI_{i_1}I_{i_2}, \widehat{\mathbf{S}}_i\right).$$

where $\widehat{\mathbf{S}}_i = \mathbf{S}_i + \sum_{t=1}^T \omega_t^{-1} \mathbf{E}_{t,(i)}(\Sigma_{i_1}^{-1} \otimes \Sigma_{i_2}^{-1}) \mathbf{E}'_{t,(i)}$, $i_1, i_2 \in \{1, 2, 3\}/i$ and $i_1 > i_2$.

4 Simulation Results

In this section, we examine the finite-sample performance of four estimators: (1) a Bayesian VAR(1) estimator with a Minnesota prior (BVAR-Minn), (2) an estimator based on CP decomposition (BTAR-CP), (3) a Tucker decomposition-based estimator (BTAR-TK), and (4) a Tucker-based estimator incorporating the multiway stick breaking shrinkage prior (BTAR-TK-MSB). We consider two experiments. In the first case, we assume a low-rank structure for the coefficient tensor, while in the second case, we assume a more general Gaussian-distributed coefficient tensor.

In the first experiment, we generate \mathcal{B} according to Equation (8), which is then used to simulate the data based on Equation (1) with $p = 1$. Each element of the core tensor \mathcal{G} follows a uniform distribution $\mathcal{U}(0, 1)$ and the marginal vectors $\mathbf{b}_i^{r_i} \sim \mathcal{N}(0.3, 0.5^2 \mathbf{I}_{I_i})$. Additionally, \mathcal{B} is normalized so that its Frobenius norm¹ is equal to 5. All entries of \mathcal{A}_0 are set to 0.1, and those of \mathcal{A}_1 are set to 0. To apply Bayesian VAR(1) estimation, we vectorize the tensor \mathcal{Y}_t by stacking its elements into a long vector. The Bayesian VAR(1) estimator is more general as it allows for more complex dynamic patterns beyond the low-rank structure. However, its main drawback is the large number of parameters to be estimated. Overall, compared to CP- and Tucker-based estimation, the BVAR(1) estimator exhibits lower bias but higher variance in finite samples, particularly when the dimensionality of the time series is high.

The DGP cases differ in dimensions—either $I_1 = I_2 = I_3 = 5$ or $I_1 = I_2 = 10, I_3 = 2$ —with average estimation errors reported for $T = 200, 300, 400, 500$ or $T = 300, 400, 500, 600$, respectively. Additionally, two Tucker rank settings are used: (1) $R_i = 2$ for all i ;

¹The Frobenius norm of a tensor \mathcal{B} is defined as $\|\mathcal{B}\| = \sqrt{\langle \mathcal{B}, \mathcal{B} \rangle}$.

(2) $(R_1, \dots, R_6) = (1, 1, 1, 2, 2, 2)$. In Case 2, since CP models cannot accommodate unequal ranks across modes, we instead include two alternative CP models with $R_i = 1$ and $R_i = 2$ for all i . We consider both dense and sparse DGPs—the latter setting the second column of \mathbf{B}_2 and \mathbf{B}_5 to zero. In total, this results in eight distinct DGPs.

Figure 2 presents the simulation results from the first experiment, showing the relative root mean squared errors (RMSEs) of low-rank models compared to the Bayesian VAR(1) model. The RMSEs for the benchmark Bayesian VAR(1) models are evaluated at $T = 500$ and $T = 600$, corresponding to the settings $I_1 = I_2 = I_3 = 5$ and $I_1 = I_2 = 10, I_3 = 2$, respectively—both of which yield the lowest RMSEs among all sample sizes considered. All low-rank models lead to lower RMSEs than the Bayesian VAR(1), and as the sample size increases, the RMSEs of all models generally decline. Notably, across both data-generating processes, model dimensions, and rank specifications, BTAR models based on Tucker decomposition consistently outperform those based on CP decomposition. Even when the rank is set to $(R_1, \dots, R_6) = (1, 1, 1, 2, 2, 2)$ where both CP models with $R_i = 1$ and $R_i = 2$ are considered, the Tucker-based model performs at least as well, if not better. Moreover, incorporating multiway stick-breaking shrinkage priors further improves the estimation accuracy for sparse DGPs, resulting in slightly lower RMSEs compared to the Tucker model without shrinkage.

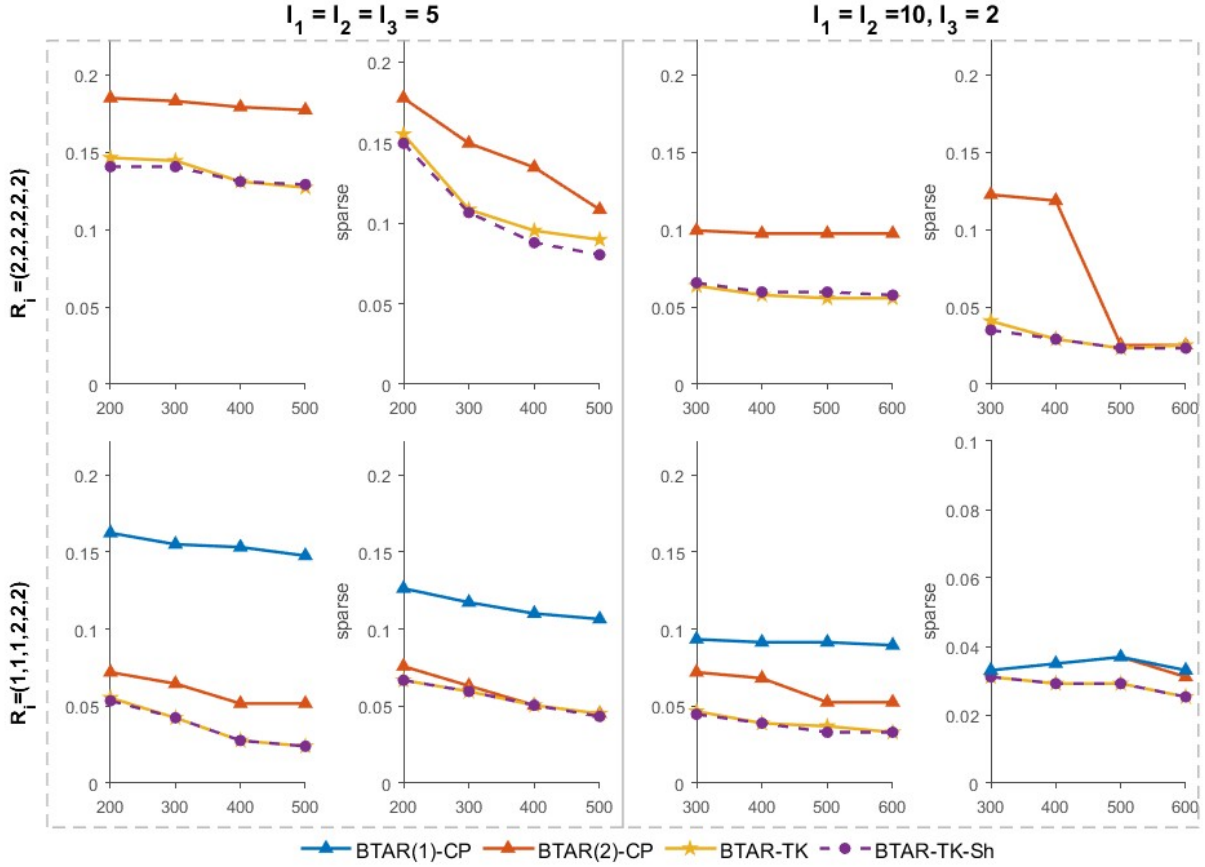


Figure 2: Relative root mean squared errors of low-rank models compared to the BVAR-Minn model

In the second experiment, we consider a more general setting by generating data from a VAR(1) model specified in Equation (5) where the off-diagonal elements of $\hat{\mathbf{B}}$ are independently drawn from a normal distribution $\mathcal{N}(0, 0.3^2)$, and the diagonal elements are drawn from a uniform distribution $U(0.1, 0.4)$. $\hat{\mathbf{B}}$ is also normalized so that its Frobenius norm is equal to 5. The error terms $\boldsymbol{\varepsilon}_t$ are generated in accordance with equation (6). We analyze both Tucker-based matrix-variate autoregressions (MAR) and tensor-variate autoregressions (TAR) with the sample size of 300 and 500. For each case, we examine two sets of dimensions. We consider $(I_1, I_2) = (3, 3)$ or $(5, 5)$ in the matrix setting, and $(I_1, I_2, I_3) = (2, 2, 2)$ or $(3, 3, 2)$ for the tensor setting.

Figure 3 shows the average estimation errors corresponding to the associated ranks on the x-axis. As the rank R increases, the estimation errors of both MAR and TAR models converge toward those of the Bayesian VAR. The Tucker-based MAR models could

even yield lower estimation errors than the Bayesian VAR(1), demonstrating the effectiveness of low-rank tensor decomposition in approximating classical methods for small to medium-sized datasets. Furthermore, the Tucker model produces similar estimation results regardless of whether shrinkage priors are applied, and consistently outperforms the CP decomposition across all configurations, highlighting its superior flexibility and generality.

It is important to emphasize that this data-generating process is particularly unfavorable to our low-rank structured models—VAR coefficients are generated independently, resulting in full-rank coefficient matrices and tensors. In contrast, our models are designed to handle low-rank structures. Nevertheless, the results suggest that our approach remains competitive, and by modestly increasing the Tucker rank, it can even outperform the Bayesian VAR in small or medium datasets.

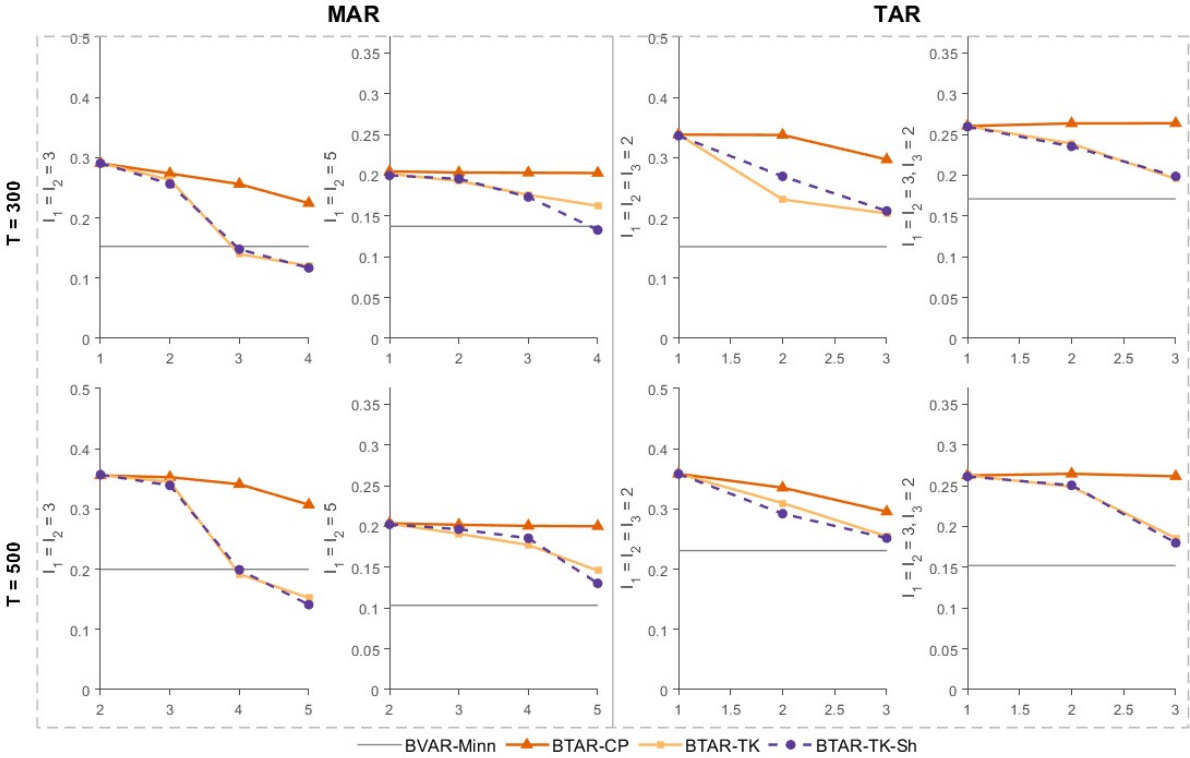


Figure 3: Root mean squared errors for competing models

5 Empirical Application

In this section, we analyze the monthly bilateral trade flow data from UN COMTRADE database. It covers 19 countries across 15 commodity categories from January 2010 to December 2023. These countries include 2 Asian countries (China, Japan), 2 North American countries (Canada, United States), a major South American country (Brazil), and 14 European countries (Belgium, Denmark, France, Germany, Ireland, Italy, Netherlands, Norway, Poland, Portugal, Spain, Sweden, Turkey, United Kingdom). Fifteen commodity groups categorize a broad range of commodities according to their two-digit Harmonized System (HS) codes, as outlined in Appendix C.

To mitigate the impact of incidental trades with unusually large or small sizes, trade values are converted into three-month moving averages and then transformed into normalized year-over-year change time series. As a result, the $19 \times 19 \times 15$ tensor, \mathcal{Y}_t , consists of 5,415 time series with a sample size of $T = 156$, spanning January 2011 to December 2023. The element $\mathcal{Y}_{t,i_1,i_2,i_3}$ represents the normalized three-month averaged change in the import value of commodity i_3 from exporting country i_2 to importing country i_1 . The coefficient $\mathcal{B}_{i_1,i_2,i_3,j_1,j_2,j_3}$ captures the effect of the lagged trade value of commodity j_3 between country j_1 and j_2 on the current trade value of commodity i_3 between country i_1 and i_2 . We choose $R_i = 4$ for all dimensions. As noted above, because the stick-breaking rank-specific priors adaptively prefer low-rank structure, we do not impose an explicit rank-selection step.

5.1 Common Stochastic Volatility

Figure 4 presents the posterior means of the error standard deviations from the BTAR-CSV model. The figure reveals several notable fluctuations, indicated by the red dotted lines, with the first spike occurring at the start of the COVID-19 pandemic in January 2020 which unleashed a global economic shock, leading to the most severe worldwide crisis in over a century, followed by a bounce-back one year later as the world recovered from the pandemic. The third jump took place in February 2022 during the onset of the Russia-Ukraine war. The conflict, along with ensuing sanctions, severely disrupted regional exports of multiple commodities—including metals, food, oil, and gas—triggering the highest inflation in decades. The final surge reflects escalated regional tensions following

the outbreak of the Israel-Hamas war in October 2023. In its aftermath, attacks in the Red Sea prompted shipping companies to avoid the Suez Canal, rerouting via the Cape of Good Hope—adding roughly 3,500 nautical miles and 14 days to voyages. This has especially disrupted trade between Europe and Asia.

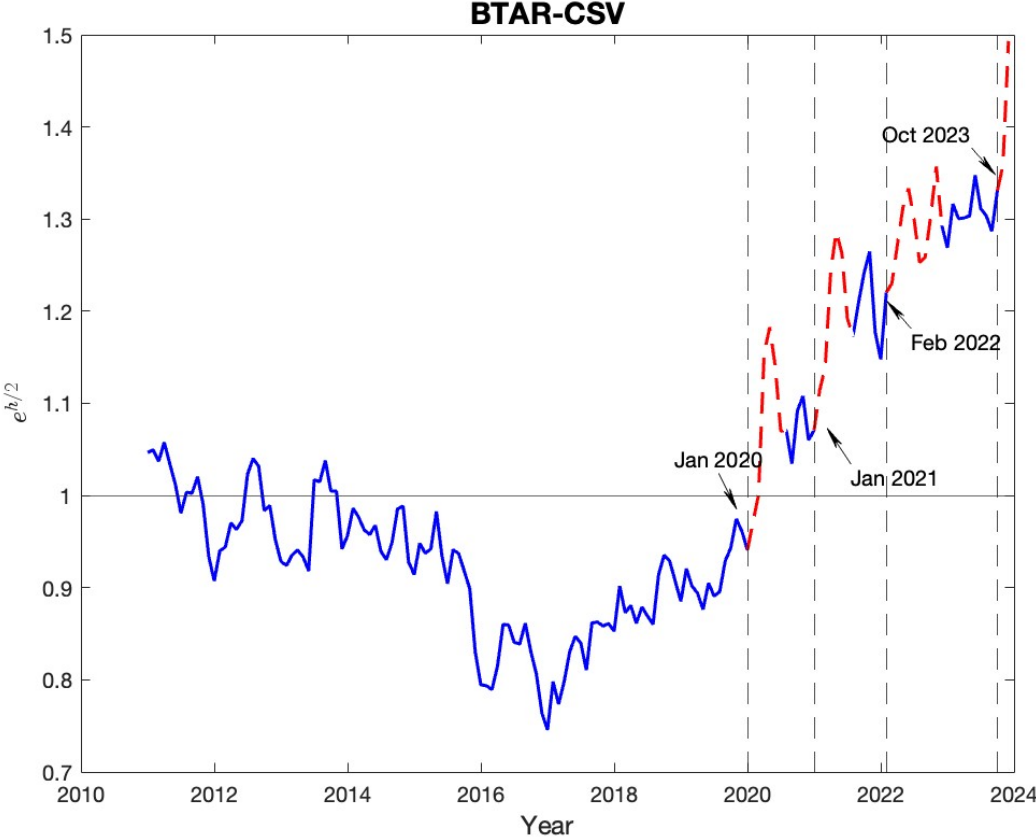


Figure 4: Posterior means of time-varying standard deviations, $exp(h_t/2)$, from BTAR-CSV model

5.2 Interpretation of \mathbf{B}_i

We can interpret the matrices $\mathbf{B}_i, i = 1, \dots, 6$, in terms of two factor analysis. Firstly, let's revisit Proportion 1. For the first equation, define a $R_1 \times I_2 I_3$ matrix $\mathbf{P}_{1t} = \mathbf{G}_{(1)} \mathbf{B}'_{-1} \mathbf{X}_{1t}$. Then, we have:

$$\mathcal{Y}_{t, \cdot, i_2, i_3} = \mathcal{A}_{t, \cdot, i_2, i_3} + \mathbf{B}_1 \mathbf{P}_{1t, \cdot, (i_3-1)I_2+i_2} + \mathcal{E}_{t, \cdot, i_2, i_3}.$$

\mathbf{B}_1 can be interpreted as the loading matrix in a standard factor model for all mode-1 fibers $\mathcal{Y}_{t, \cdot, i_2, i_3}$, across all combinations of (t, i_2, i_3) . The tensor slice $\mathcal{Y}_{t, \cdot, i_2, i_3}$ represents the import values of commodity i_3 from source country i_2 to all destination countries at time t , and is fitted using a $R_1 \times 1$ factor $\mathbf{P}_{1t, \cdot, (i_3-1)I_2+i_2}$. Similarly, \mathbf{B}_2 and \mathbf{B}_3 serve as loading matrices for the standard factor models of mode-2 fibers $\mathcal{Y}_{t, i_1, \cdot, i_3}$ and mode-3 fibers $\mathcal{Y}_{t, i_1, i_2, \cdot}$, respectively.

An alternative factor interpretation is as follows. As discussed in subsection 2.6, the HOSVD ensures that $\mathbf{B}'_i \mathbf{B}_i = \mathbf{I}_{R_i}$. Therefore, it follows from Lemma 2 that

$$\tilde{\mathbf{B}}'_m (\mathbf{y}_t - \mathbf{a}_t) = \tilde{\mathbf{G}} \tilde{\mathbf{B}}'_m \mathbf{y}_{t-1} + \tilde{\mathbf{B}}'_m \mathbf{e}_t,$$

where $\tilde{\mathbf{B}} = \mathbf{B}_6 \otimes \mathbf{B}_5 \otimes \mathbf{B}_4$, $\tilde{\mathbf{B}}_m = \mathbf{B}_3 \otimes \mathbf{B}_2 \otimes \mathbf{B}_1$, and $\tilde{\mathbf{G}}$ is an $\tilde{R}_m \times \tilde{R}$ matrix such that $\text{vec}(\tilde{\mathbf{G}}) = \text{vec}(\mathcal{G})$, with $\tilde{R}_m = R_1 R_2 R_3$ and $\tilde{R} = R_4 R_5 R_6$.

This formula allows to provide a dynamic factor interpretation on both sides. In particular, the $\tilde{R} = \prod_{i=4}^6 R_i$ lagged (predictor) factors, $\tilde{\mathbf{B}}'_m \mathbf{y}_{t-1}$, drive the dynamics of the international bilateral trade flows. Meanwhile, the current state of the trade market is captured by the $\tilde{R}_m = \prod_{i=1}^3 R_i$ response factors, $\tilde{\mathbf{B}}'_m \mathbf{y}_t$. $\tilde{\mathbf{G}}$, the matricization of compact core tensor \mathcal{G} , encapsulates the predictive relationships between these lower-dimensional predictors and responses. Specifically, each factor matrix acts as a loading matrix that projects high-dimensional predictors or responses onto a specific lower-dimensional subspace, as shown in the following equations:

$$\tilde{\mathbf{B}}'_m \mathbf{y}_t = \text{vec}(\mathbf{B}'_1 \mathbf{Y}_{t, (1)} (\mathbf{B}_3 \otimes \mathbf{B}_2))$$

and

$$\tilde{\mathbf{B}}'_m \mathbf{y}_{t-1} = \text{vec}(\mathbf{B}'_4 \mathbf{Y}_{t-1, (1)} (\mathbf{B}_6 \otimes \mathbf{B}_5))$$

In this example of the bilateral trade flows, \mathbf{B}_1 (and \mathbf{B}_4) represents the factor loading projecting the responses (or predictors) onto the import dimension. Similarly, \mathbf{B}_2 (and

\mathbf{B}_5) projects the responses (or predictors) onto the export dimension, and \mathbf{B}_3 (and \mathbf{B}_6) projects the responses (or predictors) onto the goods dimension. Figures 5 - 8 display heatmaps of the estimated loading matrices² - \mathbf{B}_i , $i = 1, 2, 4, 5$, and of the projection matrices $\mathbf{B}_i\mathbf{B}'_i$, $i = 3, 6$, from the Tucker model with hierarchical shrinkage priors on the margins. The projection matrix is identifiable, and its diagonal elements measure the total loading strength of each commodity across all factors.

Figure 5 presents the loading response matrices \mathbf{B}_1 and \mathbf{B}_2 . The left panel displays the four import hubs (I_1 - I_4) of \mathbf{B}_1 , and the right panel shows the four export hubs (E_1 - E_4) of \mathbf{B}_2 . In the import dimension, France and Germany load most heavily on I_2 and I_3 , respectively, while I_4 shows a U.S.-China nexus. The first factor, I_1 , captures a global factor with non-negligible weights across most countries. In the export dimension, E_1 again represents a global factor, whereas China, Germany, and France dominate E_2 , E_3 , and E_4 , respectively. Figure 6 depicts the response-projection matrix across commodities. Mineral products display the strongest loadings, emerging as the primary indicator of current trade dynamics. The figure further classifies commodities into two broad groups: heavy manufactured goods (including machinery and electrical equipment, transportation goods, and miscellaneous goods) and other goods.

²Note that \mathbf{B}_i is subject to sign indeterminacy in each column. We choose the sign so that the element with the largest loading in each column is positive

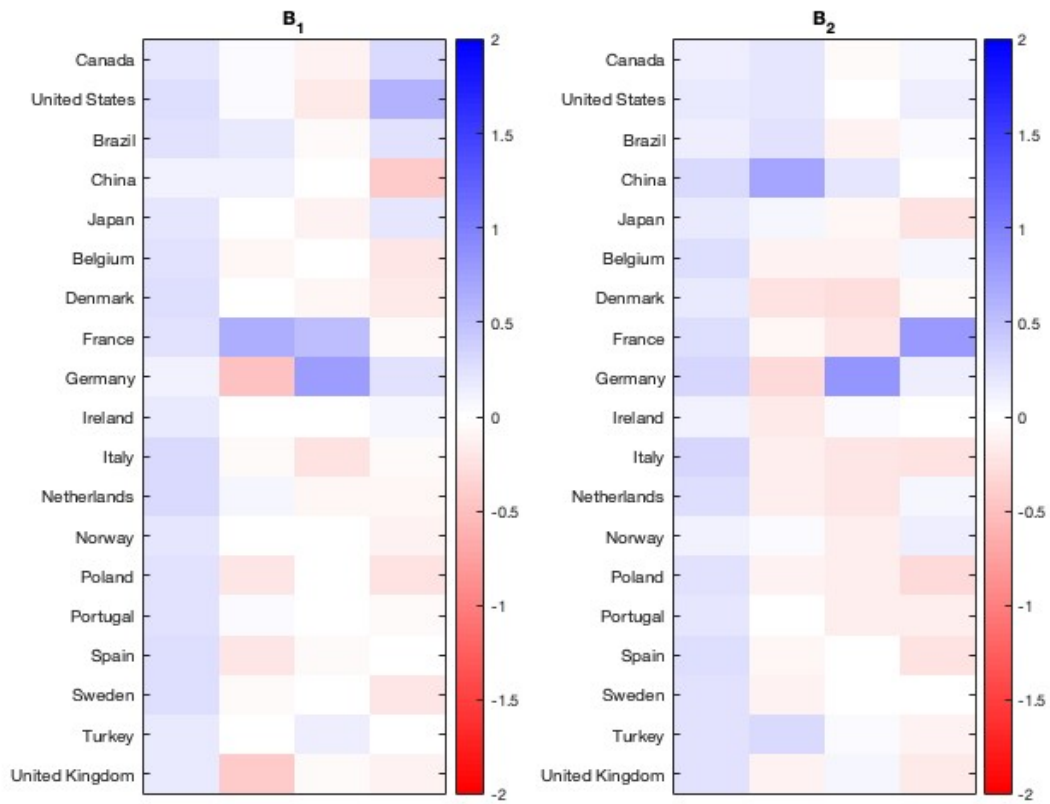


Figure 5: Heatmaps of loading matrices, B_1 and B_2

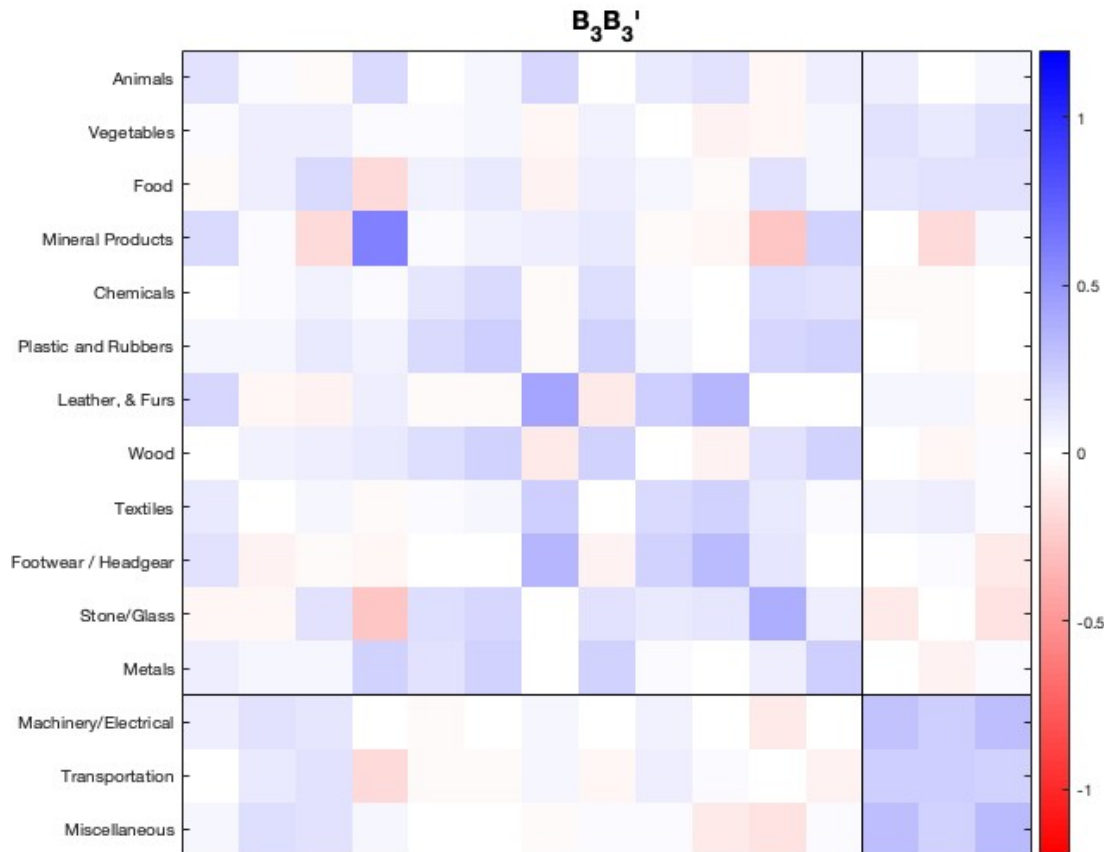


Figure 6: Heatmap of projection matrix for \mathbf{B}_3

Figure 7 illustrates the estimated loading predictor matrices, \mathbf{B}_4 (import hubs I_1 – I_4) and \mathbf{B}_5 (export hubs E_1 – E_4). In the import panel (left), I_1 captures a global import hub, while I_2 reflects U.S.–Europe linkages with relatively greater weights toward Europe. The third factor, I_3 , represents U.S.–China connections with a stronger loading on the United States, whereas I_4 characterizes a China–Europe nexus. In the export panel (right), E_1 primarily corresponds to a European factor, and E_2 – E_4 capture Europe-centered global factors. Figure 8 presents the predictor-projection heatmap across commodity categories. As mentioned earlier, the heavy loadings along a few diagonals underscore the role of manufactured goods—particularly plastics and rubber, footwear and headgear, and metals—as the principal drivers of global trade dynamics.

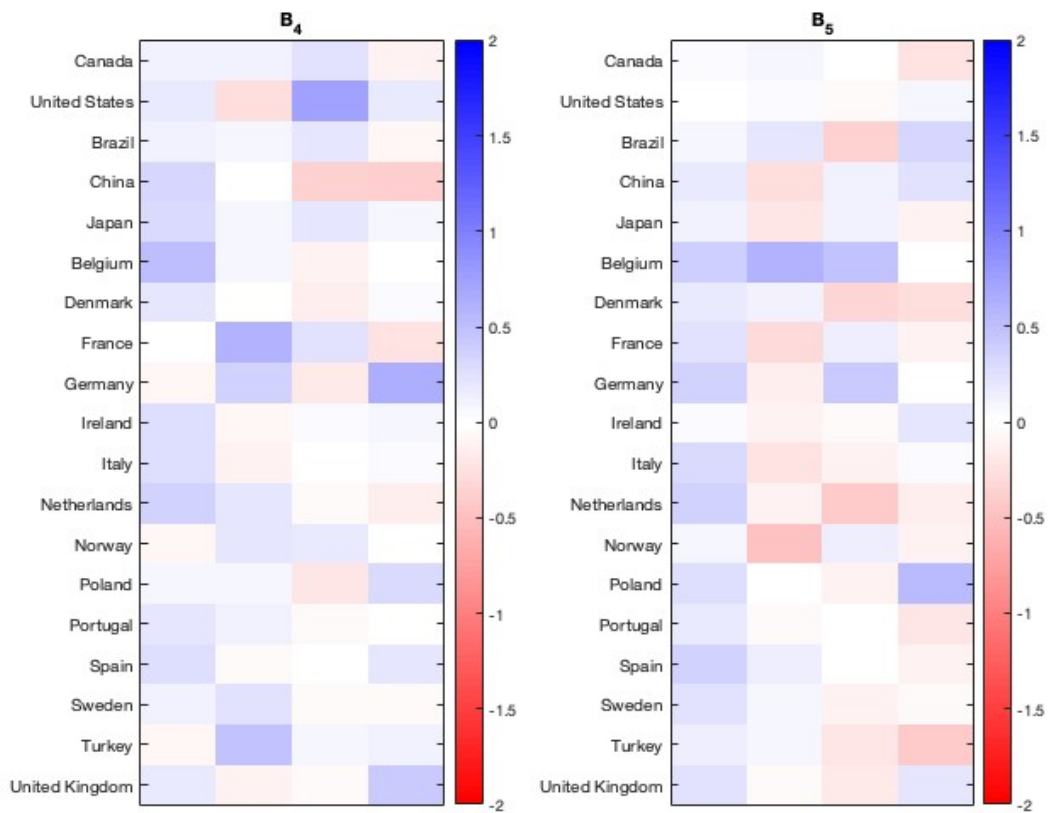


Figure 7: Heatmaps of loading matrices, B_4 and B_5

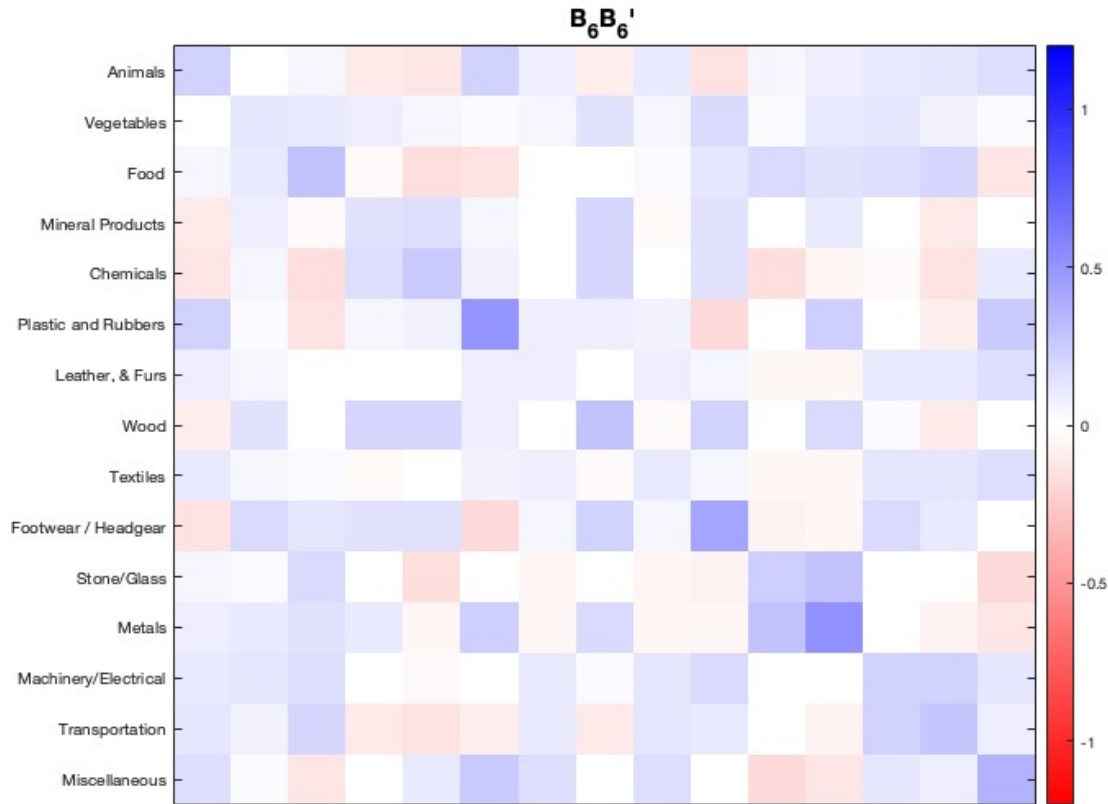


Figure 8: Heatmap of projection matrix for \mathbf{B}_6

5.3 Interpretation for Response Factor Time Series

In the BTAR-TK model with shrinkage priors, we adopt a dynamic factor interpretation for both responses and predictors. Specifically, the 64 ($= R_1 R_2 R_3 = R_4 R_5 R_6$) lagged response and predictor factor time series, $\{\tilde{\mathbf{B}}'_m \mathbf{y}_t\}$ and $\{\tilde{\mathbf{B}}' \mathbf{y}_{t-1}\}$, are constructed; in the main text we focus on the response factors. Although the model is estimated on disaggregated country- and commodity-level data, most dimension-reduced response factors closely track more aggregated global indicators; the corresponding indicators are also displayed in the figure. Because each column of \mathbf{B}_i is identified only up to sign, the sign of each factor is indeterminate; we orient each factor by choosing the sign that minimizes the RMSE with the corresponding index.

Specifically, almost each of the 64 factor series aligns with several three-month averages of standardized year-over-year growth rates of common indicators considered in Guichard and Rusticelli (2011): (1) Real Broad Dollar Index, (2) World Industrial Production Index, (3) US Export Price Index, (4) US Trade Policy Uncertainty Index, (5) PPI: Nonmetallic Mineral Products, (6) World Semiconductor Billings, (7) Brent crude oil prices, and (8) US high-yield spread.

Approximately 26.6% of the factors align with the Real Broad Dollar Index (trade-weighted U.S. dollar), followed by the World Industrial Production Index and the U.S. Export Price Index, each accounting for 15.6%. This finding is consistent with Guichard and Rusticelli (2011), who identify the World Industrial Production Index as a key driver in the initial projection period of a dynamic factor model. Brent crude oil prices aligns with 14% of the response factors, while the U.S. Trade Policy Uncertainty Index and the PPI for Nonmetallic Mineral Products each contribute 12.5%. The remaining indicators—World Semiconductor Billings (WSTS, a proxy for the global technology cycle), oil prices, the U.S. high-yield spread (capturing broader credit conditions affecting real activity and trade finance), and the U.S. Export Price Index—each account for less than 7.8%.

Figure 9 presents the 4×4 standardized response factors corresponding to four import modes and four export modes for the first commodity category. The red lines plot the factors derived from the model, while the blue lines show the corresponding aggregated indices. The other three 4×4 panels for the remaining commodity categories are provided in the appendix.

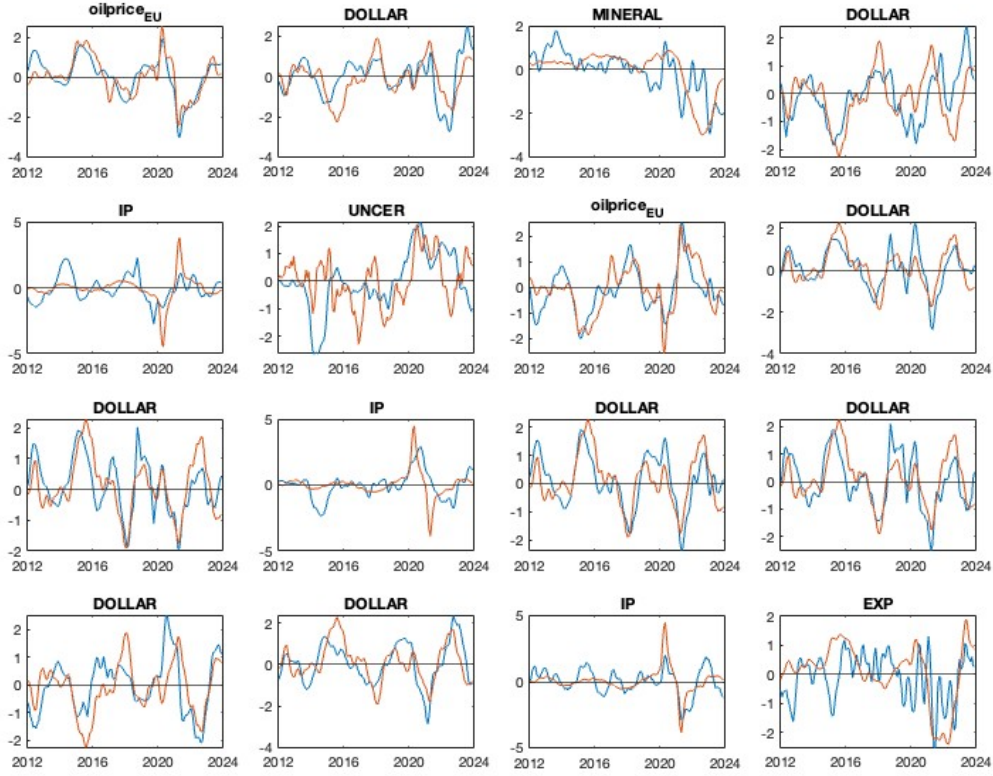


Figure 9: Response factors for $r_3 = 1$

6 Conclusion

In summary, we introduce a flexible and computationally efficient Bayesian framework for third-order tensor autoregressions based on Tucker decomposition. Our approach’s key innovations are the integration of stochastic volatility and hierarchical shrinkage priors—which automatically shrink negligible tensor coefficients toward zero—into high-dimensional tensor-on-tensor regression. In extensive MCMC experiments, we show that when the true data-generating process is low-rank, the Tucker model, especially the model with multiway stick breaking shrinkage priors, tend to outperform both CP decomposition and standard Bayesian VARs. Even if the true coefficient tensor lacks an assumed low-rank structure, our method remains competitive with Bayesian VARs on small and

medium datasets. Finally, in an empirical application to $19 \times 19 \times 15$ multi-category bilateral trade flows, we identify the principal countries and commodity groups driving global trade dynamics. We also provide a factor interpretation that links the model's factors to global indicators.

Appendix A: Proofs of Propositions

Proof of Proposition 1. I will provide the proof for $i = 1$, and the same logic can apply to other i .

Without loss of generality, we ignore the intercept term from the equations. According to Equation (10), it is equivalent to show that $\mathbf{Y}_{t,(1)} = \mathbf{B}_{(1)}\mathbf{X}_{1t} + \mathbf{E}_{t,(1)}$. Due to the redundancy of the subscript in $\mathbf{Y}_{t,(1)}$, I will represent $\mathbf{Y}_{t,(1)}$ as $\mathbf{Y}_t^{(1)}$ in this proof.

Let's start with the $(i_1, k)^{th}$ element of $\mathbf{Y}_{t,(1)}$: $\mathbf{Y}_{t,i_1,k}^{(1)}$. For any k , we can find a unique pair (i_2, i_3) such that $k = (i_3 - 1)I_2 + i_2$. By definition, $\mathbf{Y}_{t,i_1,k}^{(1)}$ corresponds to the $(i_1, i_2, i_3)^{th}$ element of \mathcal{Y}_t . Thus, $\mathbf{Y}_{t,i_1,k}^{(1)} = \mathcal{Y}_{t,i_1,i_2,i_3}$. Likewise, $\mathbf{E}_{t,i_1,k}^{(1)} = \mathcal{E}_{t,i_1,i_2,i_3}$.

As for the right equation, \mathbf{X}_{1t} is an $I_2I_3I \times I_2I_3$ matrix. The $(i_1, k)^{th}$ element of the first part in the right side is the sum of the products of the elements in the i_1^{th} row of $\mathbf{B}_{(1)}$ and the k^{th} column of \mathbf{X}_{1t} . The elements in the k^{th} column of \mathbf{X}_{1t} are given by:

$$\mathbf{X}_{1t,j,k} = \begin{cases} \mathbf{y}_{t-1,m}, & \text{if } j = k + (m-1)I_2I_3 \text{ for } m = 1, 2, \dots, I, \\ 0, & \text{otherwise.} \end{cases}$$

Thus the $(i_1, k)^{th}$ element of the first part in the right side has the following representation:

$$\begin{aligned} \sum_{j=1}^{I_2I_3I} \mathbf{B}_{(1),i_1,j} \mathbf{X}_{1t,j,k} &= \sum_{m=1}^I \mathbf{B}_{(1),i_1,k+(m-1)I_2I_3} \mathbf{X}_{1t,k+(m-1)I_2I_3,k} \\ &= \sum_{m=1}^I \mathbf{B}_{(1),i_1,(m-1)I_2I_3+(i_3-1)I_2+i_2} \mathbf{y}_{t-1,m} \end{aligned}$$

Since $\mathbf{B}_{(1),i_1,(m-1)I_2I_3+(i_3-1)I_2+i_2}$ corresponds to the $(i_1, i_2, i_3, m)^{th}$ element of \mathcal{B} by definition, the above equation can be rewritten as

$$\sum_{j=1}^{I_2I_3I} \mathbf{B}_{(1),i_1,j} \mathbf{X}_{1t,j,k} + \mathbf{E}_{t,i_1,k}^{(1)} = \sum_{m=1}^I \mathcal{B}_{i_1,i_2,i_3,m} \mathbf{y}_{t-1,m} + \mathcal{E}_{t,i_1,i_2,i_3} = \mathcal{Y}_{t,i_1,i_2,i_3}$$

This demonstrates the equality of the left and right sides of the first equation. \square

Proof of Lemma 2. To prove the first equation, we refer back to Proposition 1.

$$\mathbf{Y}_{t,(1)} - \mathbf{A}_{t,(1)} = \mathbf{B}_{(1)}(\mathbf{y}_{t-1} \otimes \mathbf{I}_{I_2 I_3}) + \mathbf{E}_{t,(1)} = \mathbf{B}_1 \mathbf{G}_{(1)} \mathbf{B}'_{-1}(\mathbf{y}_{t-1} \otimes \mathbf{I}_{I_2 I_3}) + \mathbf{E}_{t,(1)}$$

The last equality holds given equation (10). Upon vectorizing both sides, we have

$$\begin{aligned} \mathbf{y}_t - \mathbf{a}_t &= \text{vec}(\mathbf{B}_1 \mathbf{G}_{(1)} \mathbf{B}'_{-1}(\mathbf{y}_{t-1} \otimes \mathbf{I}_{I_2 I_3})) + \mathbf{e}_t \\ &= ((\mathbf{y}'_{t-1} \otimes \mathbf{I}_{I_3} \otimes \mathbf{I}_{I_2}) \mathbf{B}_{-1} \otimes \mathbf{B}_1) \text{vec}(\mathbf{G}_{(1)}) + \mathbf{e}_t \\ &= (\mathbf{y}'_{t-1} \tilde{\mathbf{B}} \otimes \mathbf{B}_3 \otimes \mathbf{B}_2 \otimes \mathbf{B}_1) \mathbf{g} + \mathbf{e}_t \\ &= (\mathbf{y}'_{t-1} \tilde{\mathbf{B}} \otimes \tilde{\mathbf{B}}_m) \text{vec}(\tilde{\mathbf{G}}) + \mathbf{e}_t = \tilde{\mathbf{B}}_m \tilde{\mathbf{G}} \tilde{\mathbf{B}}' \mathbf{y}_{t-1} + \mathbf{e}_t \end{aligned}$$

where $\tilde{\mathbf{B}} = \mathbf{B}_6 \otimes \mathbf{B}_5 \otimes \mathbf{B}_4$, $\tilde{\mathbf{B}}_m = \mathbf{B}_3 \otimes \mathbf{B}_2 \otimes \mathbf{B}_1$ and $\tilde{\mathbf{G}}$ is an $\tilde{R}_m \times \tilde{R}$ matrix satisfying $\text{vec}(\tilde{\mathbf{G}}) = \text{vec}(\mathcal{G})$, where $\tilde{R}_m = R_1 R_2 R_3$ and $\tilde{R} = R_4 R_5 R_6$.

Regarding the proof of the second equation, we have

$$\tilde{\mathbf{B}}' \mathbf{y}_{t-1} = \tilde{\mathbf{B}}' \text{vec}(\mathbf{Y}_{t-1,(1)}) = \text{vec}(\mathbf{B}'_4 \mathbf{Y}_{t-1,(1)} (\mathbf{B}_6 \otimes \mathbf{B}_5)) = ((\mathbf{B}'_6 \otimes \mathbf{B}'_5) \mathbf{Y}'_{t-1,(1)} \otimes \mathbf{I}_{R_4}) \text{vec}(\mathbf{B}'_4)$$

It follows that

$$\mathbf{y}_t = \tilde{\mathbf{B}}_m \tilde{\mathbf{G}} \tilde{\mathbf{B}}' \mathbf{y}_{t-1} + \mathbf{e}_t = \tilde{\mathbf{B}}_m \tilde{\mathbf{G}} ((\mathbf{B}'_6 \otimes \mathbf{B}'_5) \mathbf{Y}'_{t-1,(1)} \otimes \mathbf{I}_{R_4}) \text{vec}(\mathbf{B}'_4) + \mathbf{e}_t$$

□

Appendix B: Additional Estimation Details

B.1 Full conditional distribution of the hierarchical shrinkage parameters

The posterior distributions for the shrinkage parameters are given as follows.

- (1) Sampling $(\tau_i \mid \mathcal{B}_i, \Phi_i)$

$$\begin{aligned}
p(\tau_i | \mathcal{B}_i, \Phi_i, \mathbf{w}_i) &\propto p(\tau) p(\mathbf{B}_i | \tau_i, \Phi_i, \mathbf{w}_i) \propto p(\tau_i) \sum_{r_i=1}^{R_i} p(\mathbf{b}_i^{r_i} | \tau, \Phi, \mathbf{w}) \\
&\propto \tau_i^{\alpha_{\tau_i}-1} e^{-\beta_{\tau_i} \tau} \prod_{r_i=1}^{R_i} \left(\tau^{-\frac{I_i}{2}} \exp\left(-\frac{\mathbf{b}_i^{r_i'} (\phi_i^{r_i})^{-1} \mathbf{b}_i^{r_i}}{2\tau}\right) \right) \\
&\propto \tau^{\alpha_{\tau} - \frac{R_i I_i}{2} - 1} \exp\left(-\beta_{\tau} \tau - \frac{\sum_{r_i=1}^{R_i} \mathbf{b}_i^{r_i'} (\phi_i^{r_i})^{-1} \mathbf{b}_i^{r_i}}{2\tau}\right)
\end{aligned}$$

So $(\tau_i | \mathcal{B}_i, \Phi_i, \mathbf{w}_i) \sim \text{GIG}(\alpha_{\tau} - \frac{R_i I_i}{2}, 2\beta_{\tau}, \sum_{r_i=1}^{R_i} \mathbf{b}_i^{r_i'} (\phi_i^{r_i})^{-1} \mathbf{b}_i^{r_i})$

(2) Sampling $(\eta_i^r | \mathcal{B}_i, \tau_i)$

$$\begin{aligned}
p(\eta_i^r | \mathcal{B}_i, \tau_i) &\propto p(\eta_i^r) \prod_{u=r}^{R_i} p(\mathbf{b}_i^{u'} | \eta_i^r, \tau_i) \propto (1 - \eta_i^r)^{\alpha_i - 1} \prod_{u=r}^{R_i} \phi_u^{-\frac{I_i}{2}} e^{-\frac{\mathbf{b}_i^{u'} \mathbf{b}_i^u}{2\tau_i \phi_u}} \\
&\propto (1 - \eta_i^r)^{\alpha_i - \frac{(R_i - r) I_i}{2} - 1} (\eta_i^r)^{-\frac{I_i}{2}} e^{-\frac{1}{2\tau_i} \left(\sum_{u=r}^{R_i-1} \frac{\mathbf{b}_i^{u'} \mathbf{b}_i^u}{\eta_i^u \prod_{l=1}^{u-1} (1 - \eta_i^l)} + \frac{\mathbf{b}_i^{R_i'} \mathbf{b}_i^{R_i}}{\prod_{l=1}^{R_i-1} (1 - \eta_i^l)} \right)}
\end{aligned}$$

Since the posterior distribution is not available in closed form, we need to use the Metropolis-Hastings (MH) algorithm to sample ε_r . Following Guhaniyogi and Spencer (2021), we apply the random-walk MH algorithm with a normal distribution having a variance of 0.01^2 . After drawing ε , set $\phi_i^r = \eta_i^r \prod_{l=1}^{r-1} (1 - \eta_i^l)$, and set $\phi_i^R = 1 - \sum_{r=1}^{R-1} \phi_i^r$.

(3) Sampling $(\alpha_i | \varepsilon_i)$

Let the prior distribution of α_i be uniform. The posterior distribution of α_i is then expressed as:

$$p(\alpha_i | \eta_i) \propto \prod_{r=1}^{R_i} p(\eta_i^r | \alpha) \propto \alpha_i^{R_i} \prod_{r=1}^{R_i} (1 - \eta_i^r)^{\alpha_i - 1}$$

We use Griddy-Gibbs Sampler introduced in Ritter and Tanner (1992) to sample the posterior distribution of $(\alpha | \varepsilon_1, \dots, \varepsilon_6)$. Specifically, we define a grid over the interval $[0, 1]$ and compute the posterior density of α_i at each point on the grid as the weights to sample α_i .

B.2 Full conditional distribution of \mathbf{B}_2 and \mathbf{B}_3

The derivations for the conditional distributions $(\mathbf{B}'_2, \boldsymbol{\Sigma}_2 \mid \mathbf{Y}, \mathbf{B}_{-2}, \mathbf{G}_2, \boldsymbol{\Sigma}_1, \boldsymbol{\Sigma}_3)$ and $(\mathbf{B}'_3, \boldsymbol{\Sigma}_3 \mid \mathbf{Y}, \mathbf{B}_{-3}, \mathbf{G}_3, \boldsymbol{\Sigma}_1, \boldsymbol{\Sigma}_2)$ are similar to the computation of $(\mathbf{B}'_1, \boldsymbol{\Sigma}_1 \mid \mathbf{Y}, \mathbf{B}_{-1}, \mathbf{G}_1, \boldsymbol{\Sigma}_2, \boldsymbol{\Sigma}_3)$. Therefore, I will not detail the process here but will instead present the final posterior distributions.

The postetior distribution of $(\mathbf{B}'_2, \boldsymbol{\Sigma}_2 \mid \mathbf{Y}, \mathbf{B}_{-2}, \mathbf{G}_2, \boldsymbol{\Sigma}_1, \boldsymbol{\Sigma}_3)$ has the normal-inverse-Wishart distribution with parameters $\nu_2 + TI_1I_3, \widehat{\mathbf{S}}_2, \widehat{\mathbf{B}}'_2$ and $\mathbf{K}_{\mathbf{B}'_2}^{-1}$, where

$$\begin{aligned}\widehat{\mathbf{S}}_2 &= \mathbf{S}_2 + \mathbf{B}_2^0 \mathbf{V}_{\mathbf{B}_2}^{-1} \mathbf{B}_2^{0'} + \sum_{t=1}^T \omega_t^{-1} \mathbf{Y}_{t,(2)} (\boldsymbol{\Sigma}_3^{-1} \otimes \boldsymbol{\Sigma}_1^{-1}) \mathbf{Y}'_{t,(2)} - \widehat{\mathbf{B}}_2 \mathbf{K}_{\mathbf{B}'_2} \widehat{\mathbf{B}}'_2 \\ \mathbf{K}_{\mathbf{B}'_2} &= \mathbf{V}_{\mathbf{B}'_2}^{-1} + \sum_{t=1}^T \omega_t^{-1} \mathbf{G}_{(2)} \mathbf{B}'_{-2} \mathbf{X}_{2t} (\boldsymbol{\Sigma}_3^{-1} \otimes \boldsymbol{\Sigma}_1^{-1}) \mathbf{X}'_{2t} \mathbf{B}_{-2} \mathbf{G}'_{(2)}, \\ \widehat{\mathbf{B}}'_2 &= \mathbf{K}_{\mathbf{B}'_2}^{-1} \left(\mathbf{V}_{\mathbf{B}'_2}^{-1} \mathbf{B}_2^{0'} + \sum_{t=1}^T \omega_t^{-1} \mathbf{G}_{(2)} \mathbf{B}'_{-2} \mathbf{X}_{2t} (\boldsymbol{\Sigma}_3^{-1} \otimes \boldsymbol{\Sigma}_1^{-1}) \mathbf{Y}'_{t,(2)} \right)\end{aligned}$$

where $\mathbf{X}_{2t} = \mathbf{y}_{t-1} \otimes \mathbf{I}_{I_1I_3}$, of size $I_1I_3I \times I_1I_3$.

The postetior distribution of $(\mathbf{B}'_3, \boldsymbol{\Sigma}_3 \mid \mathbf{Y}, \mathbf{B}_{-3}, \mathbf{G}_3, \boldsymbol{\Sigma}_1, \boldsymbol{\Sigma}_2)$ also has the normal-inverse-Wishart distribution with parameters $\nu_3 + TI_1I_2, \widehat{\mathbf{S}}_3, \widehat{\mathbf{B}}'_3$ and $\mathbf{K}_{\mathbf{B}'_3}^{-1}$, where

$$\begin{aligned}\widehat{\mathbf{S}}_3 &= \mathbf{S}_3 + \mathbf{B}_3^0 \mathbf{V}_{\mathbf{B}_3}^{-1} \mathbf{B}_3^{0'} + \sum_{t=1}^T \omega_t^{-1} \mathbf{Y}_{t,(3)} (\boldsymbol{\Sigma}_2^{-1} \otimes \boldsymbol{\Sigma}_1^{-1}) \mathbf{Y}'_{t,(3)} - \widehat{\mathbf{B}}_3 \mathbf{K}_{\mathbf{B}'_3} \widehat{\mathbf{B}}'_3 \\ \mathbf{K}_{\mathbf{B}'_3} &= \mathbf{V}_{\mathbf{B}'_3}^{-1} + \sum_{t=1}^T \omega_t^{-1} \mathbf{G}_{(3)} \mathbf{B}'_{-3} \mathbf{X}_{3t} (\boldsymbol{\Sigma}_2^{-1} \otimes \boldsymbol{\Sigma}_1^{-1}) \mathbf{X}'_{3t} \mathbf{B}_{-3} \mathbf{G}'_{(3)}, \\ \widehat{\mathbf{B}}'_3 &= \mathbf{K}_{\mathbf{B}'_3}^{-1} \left(\mathbf{V}_{\mathbf{B}'_3}^{-1} \mathbf{B}_3^{0'} + \sum_{t=1}^T \omega_t^{-1} \mathbf{G}_{(3)} \mathbf{B}'_{-3} \mathbf{X}_{3t} (\boldsymbol{\Sigma}_2^{-1} \otimes \boldsymbol{\Sigma}_1^{-1}) \mathbf{Y}'_{t,(3)} \right)\end{aligned}$$

where $\mathbf{X}_{3t} = \mathbf{y}_{t-1} \otimes \mathbf{I}_{I_1I_2}$, of size $I_1I_2I \times I_1I_2$.

B.3 Full conditional distribution of \mathbf{B}_5 and \mathbf{B}_6

In the following, we explore the posterior distributions for \mathbf{B}_5 and \mathbf{B}_6 . The case of \mathbf{B}_5 is more intricate, and we start by presenting a relevant lemma and proposition.

Lemma 3.

$$\tilde{\mathbf{B}}' \mathbf{y}_{t-1} = (\mathbf{P}'(\mathbf{B}'_5 \otimes \mathbf{B}'_6) \otimes \mathbf{B}'_4) \text{vec}(\mathbf{Y}'_{t-1,(2)}) \quad (16)$$

where \mathbf{P} is an $R_5 R_6 \times R_5 R_6$ commutation matrix with $\mathbf{P}_{k,q} = 1$ if there exist r_5 and r_6 such that $k = (r_5 - 1)R_6 + r_6$ and $q = (r_6 - 1)R_5 + r_5$; otherwise, $\mathbf{P}_{k,q} = 0$.

Proof. Let's look at the j^{th} element on both sides. There exists a set of (j_1, j_2, j_3) such that $j = (j_3 - 1)R_4 R_5 + (j_2 - 1)R_4 + j_1$. The j^{th} element on the left-hand side is given by

$$\begin{aligned} \sum_{i=1}^I (\tilde{\mathbf{B}}')_{j,i} \mathbf{y}_{t-1,i} &= \sum_{i_1=1}^{I_1} \sum_{i_2=1}^{I_2} \sum_{i_3=1}^{I_3} \tilde{\mathbf{B}}_{(i_3-1)I_1 I_2 + (i_2-1)I_1 + i_1, (j_3-1)R_4 R_5 + (j_2-1)R_4 + j_1} \\ &\quad \times \mathbf{y}_{t-1, (i_3-1)I_1 I_2 + (i_2-1)I_1 + i_1} \\ &= \sum_{i_1=1}^{I_1} \sum_{i_2=1}^{I_2} \sum_{i_3=1}^{I_3} \mathbf{B}_{4,i_1,j_1} \mathbf{B}_{5,i_1,j_2} \mathbf{B}_{6,i_3,j_3} \mathcal{Y}_{t-1,i_1,i_2,i_3} \end{aligned}$$

As for the right side, assuming $m = (m_2 - 1)I_3 + m_3$, and $l = (l_3 - 1)R_5 + l_2$, the $(m, l)^{\text{th}}$ element of $(\mathbf{B}_5 \otimes \mathbf{B}_6)\mathbf{P}$ is given by

$$\begin{aligned} \sum_{o=1}^{R_5 R_6} (\mathbf{B}_5 \otimes \mathbf{B}_6)_{m,o} \mathbf{P}_{o,l} &= \sum_{o_2=1}^{R_5} \sum_{o_3=1}^{R_6} (\mathbf{B}_5 \otimes \mathbf{B}_6)_{(m_2-1)I_3 + m_3, (o_2-1)R_6 + o_3} \mathbf{P}_{(o_2-1)R_6 + o_3, l} \\ &= \sum_{o_2=1}^{R_5} \sum_{o_3=1}^{R_6} \mathbf{B}_{5,m_2,o_2} \mathbf{B}_{6,m_3,o_3} \mathbf{P}_{(o_2-1)R_6 + o_3, (l_3-1)R_5 + l_2} = \mathbf{B}_{5,m_2,l_2} \mathbf{B}_{6,m_3,l_3} \end{aligned} \quad (17)$$

The last equality holds due to the definition of \mathbf{P} . As for $\text{vec}(\mathbf{Y}'_{t-1,(2)})$, the u^{th} element, where $u = (u_2 - 1)I_1 I_3 + (u_3 - 1)I_1 + u_1$, corresponds to $\mathcal{Y}_{t-1,u_1,u_2,u_3}$.

Accordingly, the j^{th} element of the right side can be represented as follows:

$$\begin{aligned}
\sum_{u=1}^I (\mathbf{P}'(\mathbf{B}'_5 \otimes \mathbf{B}'_6) \otimes \mathbf{B}'_4)_{j,u} \text{vec}(\mathbf{Y}'_{t-1,(2)})_u &= \sum_{u=1}^I ((\mathbf{B}_5 \otimes \mathbf{B}_6)\mathbf{P}) \otimes \mathbf{B}_4)_{u,j} \text{vec}(\mathbf{Y}'_{t-1,(2)})_u \\
&= \sum_{u_1=1}^{I_1} \sum_{u_2=1}^{I_2} \sum_{u_3=1}^{I_3} ((\mathbf{B}_5 \otimes \mathbf{B}_6)\mathbf{P}) \otimes \mathbf{B}_4)_{(u_2-1)I_1 I_3 + (u_3-1)I_1 + u_1, j} \\
&\quad \times \text{vec}(\mathbf{Y}'_{t-1,(2)})_{(u_2-1)I_1 I_3 + (u_3-1)I_1 + u_1} \\
&= \sum_{u_1=1}^{I_1} \sum_{u_2=1}^{I_2} \sum_{u_3=1}^{I_3} ((\mathbf{B}_5 \otimes \mathbf{B}_6)\mathbf{P})_{(u_2-1)I_3 + u_3, (j_3-1)R_5 + j_2} \mathbf{B}_{4,u_1,j_1} \mathcal{Y}_{t-1,u_1,u_2,u_3} \\
&= \sum_{u_1=1}^{I_1} \sum_{u_2=1}^{I_2} \sum_{u_3=1}^{I_3} (\mathbf{B}_{5,u_2,j_2} \mathbf{B}_{6,u_3,j_3}) \mathbf{B}_{4,u_1,j_1} \mathcal{Y}_{t-1,u_1,u_2,u_3}
\end{aligned}$$

The last equality follows the equation (17), thus establishing equivalence between the left and right sides. Proof concluded. \square

Proposition 2.

$$\mathbf{y}_t - \mathbf{a}_t = \tilde{\mathbf{B}}_m \tilde{\mathbf{G}}(\mathbf{P}'(\mathbf{I}_{R_5} \otimes \mathbf{B}'_6) \otimes \mathbf{B}'_4)(\mathbf{I}_{R_5} \otimes \mathbf{Y}'_{t-1,(2)}) \text{vec}(\mathbf{B}_5) + \mathbf{e}_t \quad (18)$$

Proof. Based on Lemma 3, it follows that

$$\begin{aligned}
\tilde{\mathbf{B}}' \mathbf{y}_{t-1} &= (\mathbf{P}'(\mathbf{B}'_5 \otimes \mathbf{B}'_6) \otimes \mathbf{B}'_4) \text{vec}(\mathbf{Y}'_{t-1,(2)}) \\
&= (\mathbf{P}' \otimes \mathbf{I}_{R_4})(\mathbf{B}'_5 \otimes \mathbf{B}'_6 \otimes \mathbf{B}'_4) \text{vec}(\mathbf{Y}'_{t-1,(2)}) \\
&= (\mathbf{P}' \otimes \mathbf{I}_{R_4}) \text{vec}(((\mathbf{B}'_6 \otimes \mathbf{B}'_4)\mathbf{Y}'_{t-1,(2)}\mathbf{B}_5)) \\
&= (\mathbf{P}' \otimes \mathbf{I}_{R_4})(\mathbf{I}_{R_5} \otimes (\mathbf{B}'_6 \otimes \mathbf{B}'_4)\mathbf{Y}'_{t-1,(2)}) \text{vec}(\mathbf{B}_5) \\
&= (\mathbf{P}' \otimes \mathbf{I}_{R_4})(\mathbf{I}_{R_5} \otimes \mathbf{B}'_6 \otimes \mathbf{B}'_4)(\mathbf{I}_{R_5} \otimes \mathbf{Y}'_{t-1,(2)}) \text{vec}(\mathbf{B}_5)
\end{aligned}$$

Then,

$$\begin{aligned}
\mathbf{y}_t &= \tilde{\mathbf{B}}_m \tilde{\mathbf{G}} \tilde{\mathbf{B}}' \mathbf{y}_{t-1} + \mathbf{e}_t = \tilde{\mathbf{B}}_m \tilde{\mathbf{G}}(\mathbf{P}' \otimes \mathbf{I}_{R_4})(\mathbf{I}_{R_5} \otimes \mathbf{B}'_6 \otimes \mathbf{B}'_4)(\mathbf{I}_{R_5} \otimes \mathbf{Y}'_{t-1,(2)}) \text{vec}(\mathbf{B}_5) + \mathbf{e}_t \\
&= \tilde{\mathbf{B}}_m \tilde{\mathbf{G}}(\mathbf{P}'(\mathbf{I}_{R_5} \otimes \mathbf{B}'_6) \otimes \mathbf{B}'_4)(\mathbf{I}_{R_5} \otimes \mathbf{Y}'_{t-1,(2)}) \text{vec}(\mathbf{B}_5) + \mathbf{e}_t
\end{aligned}$$

\square

Suppose the prior on $\text{vec}(\mathbf{B}'_5)$ is given by $\text{vec}(\mathbf{B}'_5) \sim \mathcal{N}(\mathbf{b}_5^0, \mathbf{V}_{\mathbf{b}_5})$, where \mathbf{b}_5^0 is a vector of length $I_2 R_5$, and $\mathbf{V}_{\mathbf{b}_5}$ is an $I_2 R_5 \times I_2 R_5$ diagonal matrix. Then the posterior distribution of $\text{vec}(\mathbf{B}'_5)$ is as follows:

$$\text{vec}(\mathbf{B}'_5) | \mathbf{Y}, \tilde{\mathbf{B}}_m, \mathbf{B}_4, \mathbf{B}_6, \tilde{\mathbf{G}}, \Sigma \sim \mathcal{N}(\hat{\mathbf{b}}_5, \mathbf{K}_{\mathbf{b}_5}^{-1})$$

where

$$\begin{aligned} \mathbf{K}_{\mathbf{b}_5} = & \mathbf{V}_{\mathbf{b}_5}^{-1} + \sum_{t=1}^T \frac{1}{\omega_t} (\mathbf{I}_{R_5} \otimes \mathbf{Y}_{t-1,(2)}) ((\mathbf{I}_{R_5} \otimes \mathbf{B}_6) \mathbf{P} \otimes \mathbf{B}_4) \tilde{\mathbf{G}}' \tilde{\mathbf{B}}'_m \Sigma^{-1} \tilde{\mathbf{B}}_m \tilde{\mathbf{G}} \\ & \times (\mathbf{P}' (\mathbf{I}_{R_5} \otimes \mathbf{B}'_6) \otimes \mathbf{B}'_4) (\mathbf{I}_{R_5} \otimes \mathbf{Y}'_{t-1,(2)}) \end{aligned}$$

$$\hat{\mathbf{b}}_5 = \mathbf{K}_{\mathbf{b}_5}^{-1} \left(\mathbf{V}_{\mathbf{b}_5}^{-1} \mathbf{b}_5^0 + \sum_{t=1}^T \frac{1}{\omega_t} (\mathbf{I}_{R_5} \otimes \mathbf{Y}_{t-1,(2)}) ((\mathbf{I}_{R_5} \otimes \mathbf{B}_6) \mathbf{P} \otimes \mathbf{B}_4) \tilde{\mathbf{G}}' \tilde{\mathbf{B}}'_m \Sigma^{-1} \mathbf{y}_t \right)$$

Finally, suppose the prior on $\text{vec}(\mathbf{B}'_6)$ is given by $\text{vec}(\mathbf{B}'_6) \sim \mathcal{N}(\mathbf{b}_6^0, \mathbf{V}_{\mathbf{b}_6})$, where \mathbf{b}_6^0 is an $I_3 R_6$ dimensional vector, and $\mathbf{V}_{\mathbf{b}_6}$ is an $I_3 R_6 \times I_3 R_6$ diagonal matrix. Then the posterior distribution of $\text{vec}(\mathbf{B}'_6)$ is as follows:

$$\text{vec}(\mathbf{B}'_6) | \mathbf{Y}, \tilde{\mathbf{B}}_m, \mathbf{B}_4, \mathbf{B}_5, \tilde{\mathbf{G}}, \Sigma \sim \mathcal{N}(\hat{\mathbf{b}}_6, \mathbf{K}_{\mathbf{b}_6}^{-1})$$

where

$$\begin{aligned} \mathbf{K}_{\mathbf{b}_6} = & \mathbf{V}_{\mathbf{b}_6}^{-1} + \sum_{t=1}^T \frac{1}{\omega_t} (\mathbf{I}_{R_6} \otimes \mathbf{Y}_{t-1,(3)} (\mathbf{B}_5 \otimes \mathbf{B}_4)) \tilde{\mathbf{G}}' \tilde{\mathbf{B}}'_m \Sigma^{-1} \tilde{\mathbf{B}}_m \tilde{\mathbf{G}} (\mathbf{I}_{R_6} \otimes (\mathbf{B}'_5 \otimes \mathbf{B}'_4) \mathbf{Y}'_{t-1,(3)}) \\ \hat{\mathbf{b}}_6 = & \mathbf{K}_{\mathbf{b}_6}^{-1} \left(\mathbf{V}_{\mathbf{b}_6}^{-1} \mathbf{b}_6^0 + \sum_{t=1}^T \frac{1}{\omega_t} (\mathbf{I}_{R_6} \otimes \mathbf{Y}_{t-1,(3)} (\mathbf{B}_5 \otimes \mathbf{B}_4)) \tilde{\mathbf{G}}' \tilde{\mathbf{B}}'_m \Sigma^{-1} \mathbf{y}_t \right) \end{aligned}$$

Appendix C: Data Description

The fifteen commodity groups include all two-digit HS categories: Animal and Animal Products (HS01–HS05), Vegetable Products (HS06–HS15), Foodstuffs (HS16–HS24), Mineral Products (HS25–HS27), Chemicals and Allied Industries (HS28–HS38), Plas-

tics and Rubbers (HS39, HS40), Raw Hides, Skins, Leather, and Furs (HS41–HS43), Wood and Wood Products (HS44–HS49), Textiles (HS50–HS63), Footwear and Headgear (HS64–HS67), Stone and Glass (HS68–HS71), Metals (HS72–HS83), Machinery and Electrical (HS84, HS85), Transportation (HS86–HS89), and Miscellaneous (HS90–HS97).

Appendix D: Additional Response and Predictor Factors

Below are the remaining three panels of response factor time series.

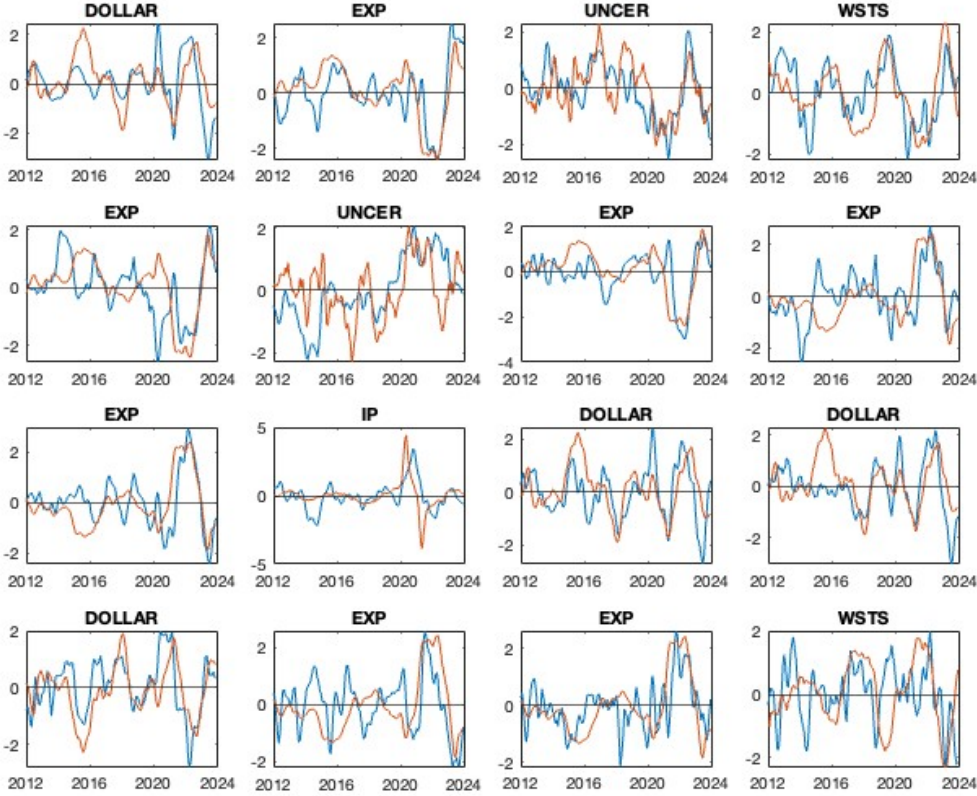


Figure 10: Response factors for $r_3 = 2$

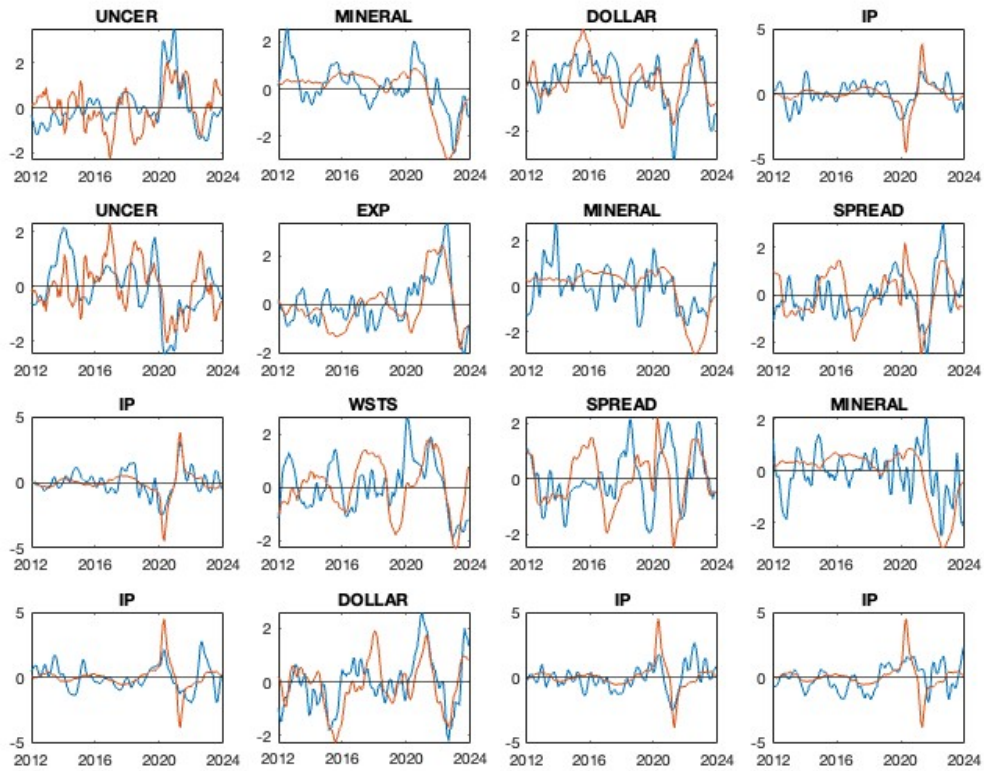


Figure 11: Response factors for $r_3 = 3$

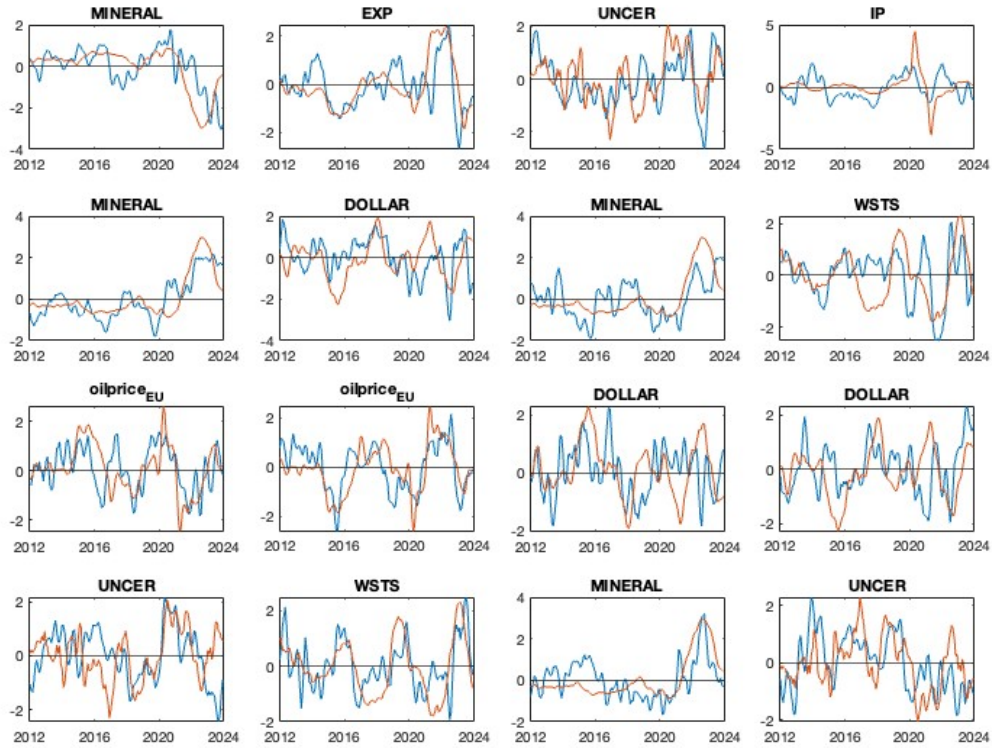


Figure 12: Response factors for $r_3 = 4$

Figures 13–16 display four 4×4 panels of standardized predictor factors. Nearly all series align with the three-month averages of standardized year-over-year growth in one of the following indicators: (1) World Industrial Production Index, (2) Real Broad Dollar Index, (3) PPI: Nonmetallic Mineral Products, (4) U.S. Export Price Index, (5) Brent crude oil prices, (6) U.S. Trade Policy Uncertainty Index, (7) World Semiconductor Billings (WSTS), and (8) U.S. high-yield spread. In each panel, the red lines represent the model-derived factors, while the blue lines denote the corresponding aggregate indices.

More than 18% of the factors correspond to the World Industrial Production Index and the Real Broad Dollar Index, followed by the PPI for Nonmetallic Mineral Products (15.6%), the U.S. Export Price Index (14.1%), and Brent crude oil prices (10.9%). Approximately 7.8% of the predictor factors are associated with either the U.S. Trade Policy Uncertainty Index or WSTS, while the remaining indicator—the U.S. high-yield spread—accounts for 6.25%.

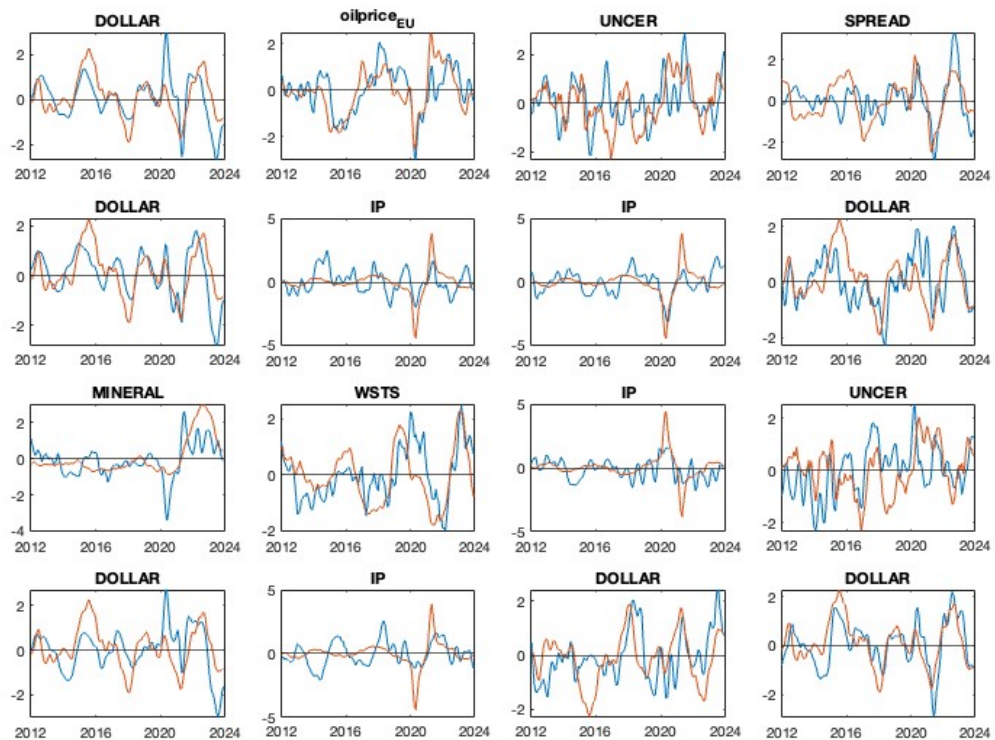


Figure 13: Predictor factors for $r_3 = 1$

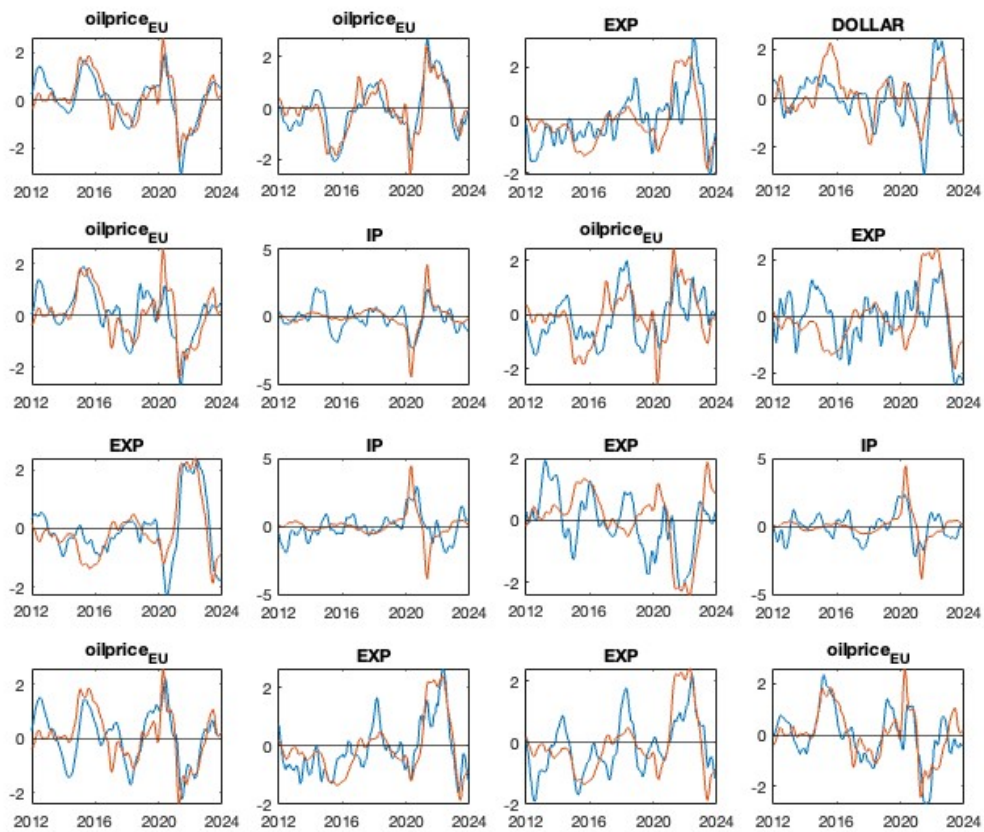


Figure 14: Predictor factors for $r_3 = 2$

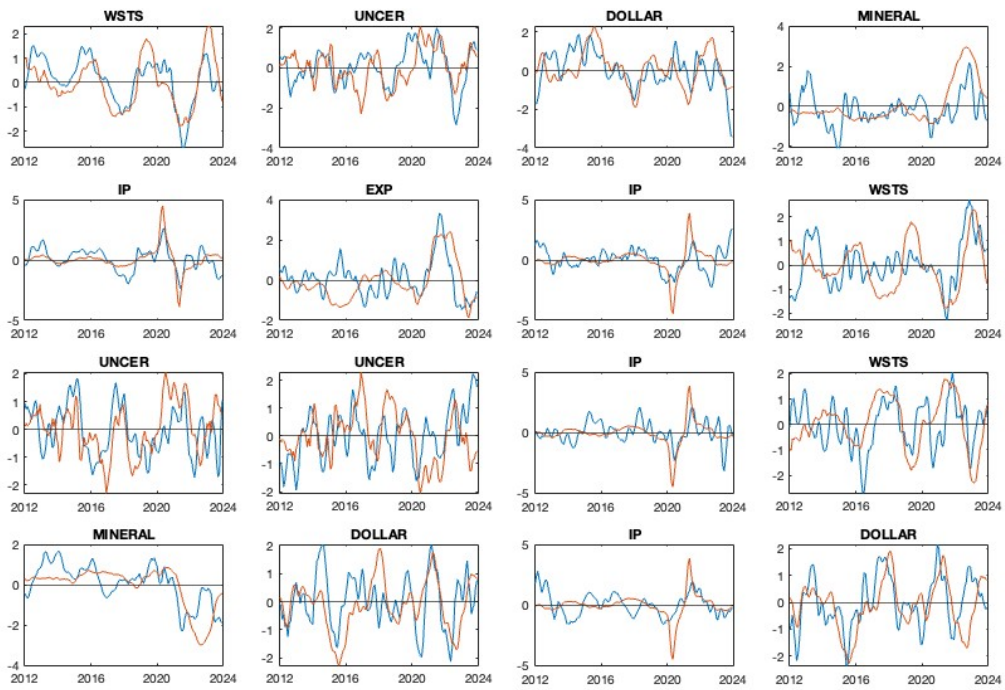


Figure 15: Predictor factors for $r_3 = 3$

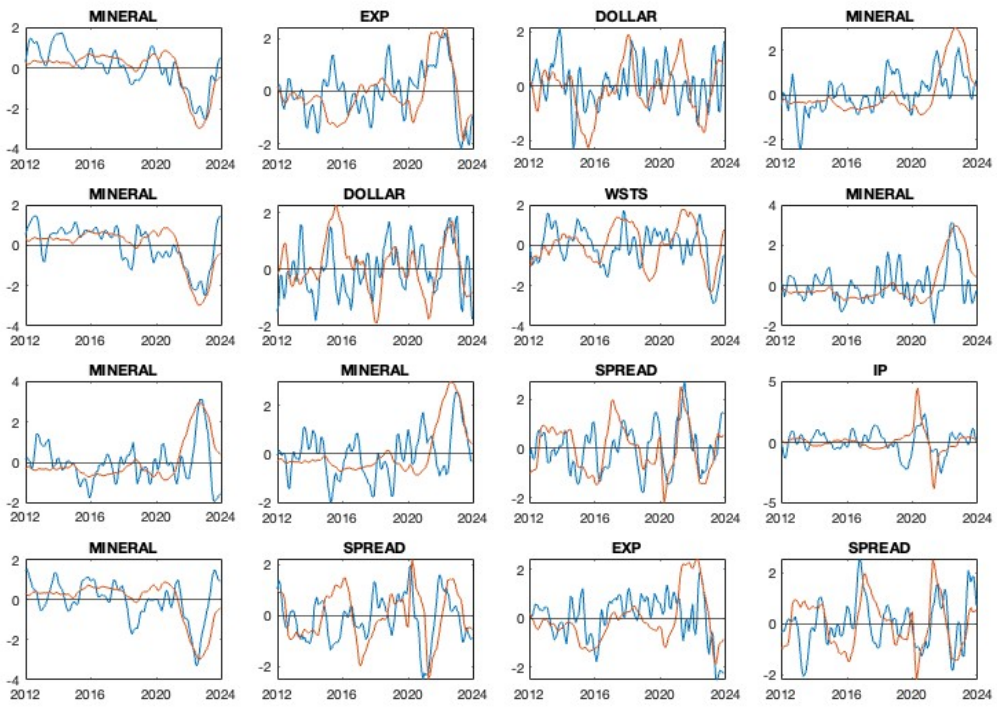


Figure 16: Predictor factors for $r_3 = 4$

References

- BAÑBURA, M., D. GIANNONE, AND L. REICHLIN (2010): “Large Bayesian vector autoregressions,” *Journal of applied Econometrics*, 25(1), 71–92.
- BILLIO, M., R. CASARIN, M. IACOPINI, AND S. KAUFMANN (2023): “Bayesian dynamic tensor regression,” *Journal of Business & Economic Statistics*, 41(2), 429–439.
- BUSSIÈRE, M., A. CHUDI, AND G. SESTIERI (2009): “Modelling global trade flows: results from a GVAR model,” Discussion paper, ECB working paper.
- CANOVA, F., AND M. CICCARELLI (2013): “Panel Vector Autoregressive Models: A Survey The views expressed in this article are those of the authors and do not necessarily reflect those of the ECB or the Eurosystem.,” in *VAR models in macroeconomics—new developments and applications: Essays in honor of Christopher A. Sims*, pp. 205–246. Emerald Group Publishing Limited.
- CARRIERO, A., T. E. CLARK, AND M. MARCELLINO (2016a): “Common drifting volatility in large Bayesian VARs,” *Journal of Business & Economic Statistics*, 34(3), 375–390.
- CARRIERO, A., T. E. CLARK, M. MARCELLINO, AND E. MERTENS (2022): “Addressing COVID-19 outliers in BVARs with stochastic volatility,” *The Review of Economics and Statistics*, Forthcoming.
- CARRIERO, A., T. E. CLARK, AND M. G. MARCELLINO (2015): “Bayesian VARs: Specification Choices and Forecast Accuracy,” *Journal of Applied Econometrics*, 30(1), 46–73.
- (2016b): “Common drifting volatility in large Bayesian VARs,” *Journal of Business and Economic Statistics*, 34(3), 375–390.
- (2019): “Large Bayesian vector autoregressions with stochastic volatility and non-conjugate priors,” *Journal of Econometrics*, 212(1), 137–154.
- CARROLL, J. D., AND J.-J. CHANG (1970): “Analysis of individual differences in multidimensional scaling via an N-way generalization of “Eckart-Young” decomposition,” *Psychometrika*, 35(3), 283–319.
- CHAN, J. C. (2023): “Comparing stochastic volatility specifications for large Bayesian VARs,” *Journal of Econometrics*, 235(2), 1419–1446.
- CHAN, J. C., E. EISENSTAT, C. HOU, AND G. KOOP (2020): “Composite likelihood methods for large Bayesian VARs with stochastic volatility,” *Journal of Applied Econometrics*, 35(6), 692–711.

- CHAN, J. C., AND Y. QI (2025): “Large Bayesian matrix autoregressions,” *Journal of Econometrics*, p. 105955.
- CHEN, E. Y., R. S. TSAY, AND R. CHEN (2020): “Constrained factor models for high-dimensional matrix-variate time series,” *Journal of the American Statistical Association*.
- CHEN, R., H. XIAO, AND D. YANG (2021): “Autoregressive models for matrix-valued time series,” *Journal of Econometrics*, 222(1), 539–560.
- COGLEY, T., AND T. J. SARGENT (2005): “Drifts and volatilities: Monetary policies and outcomes in the post WWII US,” *Review of Economic Dynamics*, 8(2), 262–302.
- DE LATHAUWER, L., B. DE MOOR, AND J. VANDEWALLE (2000): “A multilinear singular value decomposition,” *SIAM journal on Matrix Analysis and Applications*, 21(4), 1253–1278.
- DEES, S., F. D. MAURO, M. H. PESARAN, AND L. V. SMITH (2007): “Exploring the international linkages of the euro area: a global VAR analysis,” *Journal of applied econometrics*, 22(1), 1–38.
- DING, S., AND R. DENNIS COOK (2018): “Matrix variate regressions and envelope models,” *Journal of the Royal Statistical Society Series B: Statistical Methodology*, 80(2), 387–408.
- GUHANIYOGI, R. (2020): “Bayesian methods for tensor regression,” *Wiley StatsRef: Statistics Reference Online*, pp. 1–18.
- GUHANIYOGI, R., S. QAMAR, AND D. B. DUNSON (2017): “Bayesian tensor regression,” *Journal of Machine Learning Research*, 18(79), 1–31.
- GUHANIYOGI, R., AND D. SPENCER (2021): “Bayesian tensor response regression with an application to brain activation studies,” *Bayesian Analysis*, 16(4), 1221–1249.
- GUICHARD, S., AND E. RUSTICELLI (2011): “A dynamic factor model for world trade growth,” .
- HARSHMAN, R. A., ET AL. (1970): “Foundations of the PARAFAC procedure: Models and conditions for an “explanatory” multi-modal factor analysis,” *UCLA working papers in phonetics*, 16(1), 84.
- HOFF, P. D. (2015): “Multilinear tensor regression for longitudinal relational data,” *The Annals of Applied Statistics*, 9(3), 1169.
- KOLDA, T. G., AND B. W. BADER (2009): “Tensor decompositions and applications,” *SIAM review*, 51(3), 455–500.

- KOOP, G. (2013): “Forecasting with medium and large Bayesian VARs,” *Journal of Applied Econometrics*, 28(2), 177–203.
- KOOP, G., AND D. KOROBILIS (2013): “Large time-varying parameter VARs,” *Journal of Econometrics*, 177(2), 185–198.
- LEVIN, J. (1965): “Three-mode factor analysis.,” *Psychological Bulletin*, 64(6), 442.
- LI, X., D. XU, H. ZHOU, AND L. LI (2018): “Tucker tensor regression and neuroimaging analysis,” *Statistics in Biosciences*, 10(3), 520–545.
- LOCK, E. F. (2018): “Tensor-on-tensor regression,” *Journal of Computational and Graphical Statistics*, 27(3), 638–647.
- PESARAN, M. H., T. SCHUERMAN, AND S. M. WEINER (2004): “Modeling regional interdependencies using a global error-correcting macroeconomic model,” *Journal of Business & Economic Statistics*, 22(2), 129–162.
- RABUSSEAU, G., AND H. KADRI (2016): “Low-rank regression with tensor responses,” *Advances in Neural Information Processing Systems*, 29.
- RITTER, C., AND M. A. TANNER (1992): “Facilitating the Gibbs sampler: the Gibbs stopper and the gridy-Gibbs sampler,” *Journal of the American Statistical Association*, 87(419), 861–868.
- SIMS, C. A., AND T. ZHA (2006): “Were There Regime Switches in U.S. Monetary Policy?,” *American Economic Review*, 96(1), 54–81.
- SPENCER, D., R. GUHANIYOGI, AND R. PRADO (2020): “Joint Bayesian estimation of voxel activation and inter-regional connectivity in fMRI experiments,” *psychometrika*, 85(4), 845–869.
- STOCK, J. H., AND M. W. WATSON (2016): “Core inflation and trend inflation,” *Review of Economics and Statistics*, 98(4), 770–784.
- TUCKER, L. R. (1963): “Implications of factor analysis of three-way matrices for measurement of change,” *Problems in measuring change*, 15(122-137), 3.
- (1966): “Some mathematical notes on three-mode factor analysis,” *Psychometrika*, 31(3), 279–311.
- WANG, D., X. LIU, AND R. CHEN (2019): “Factor models for matrix-valued high-dimensional time series,” *Journal of econometrics*, 208(1), 231–248.
- WANG, D., Y. ZHENG, AND G. LI (2024): “High-dimensional low-rank tensor autoregressive time series modeling,” *Journal of Econometrics*, 238(1), 105544.

- WANG, K., AND Y. XU (2024): “Bayesian tensor-on-tensor regression with efficient computation,” *Statistics and its Interface*, 17(2), 199.
- ZHANG, W. (2024): “Bayesian Dynamic Factor Models for High-dimensional Matrix-valued Time Series,” *arXiv preprint arXiv:2409.08354*.
- ZHOU, H., L. LI, AND H. ZHU (2013): “Tensor regression with applications in neuroimaging data analysis,” *Journal of the American Statistical Association*, 108(502), 540–552.
- ZHOU, J., A. BHATTACHARYA, A. H. HERRING, AND D. B. DUNSON (2015): “Bayesian factorizations of big sparse tensors,” *Journal of the American Statistical Association*, 110(512), 1562–1576.